Half-title page, prepared by publisher

Publishers' page

Full title page, prepared by publisher

Copyright page, prepared by publisher

Chapter 1

Hyperonization in Compact Stars

Armen Sedrakian

Frankfurt Institute for Advanced Studies
Ruth-Moufang-Str. 1, 60438 Frankfurt am Main, Germany
Institute of Theoretical Physics
University of Wrocław
pl. M. Borna 9, 50-204 Wrocław, Poland
E-mail: sedrakian@fias.uni-frankfurt.de

Jia-Jie Li
School of Physical Science and Technology
Southwest University
Chongqing 400700, China
E-mail: jiajieli@swu.edu.cn

Fridolin Weber

Department of Physics, San Diego State University San Diego, CA 92182, USA Center for Astrophysics and Space Sciences University of California at San Diego La Jolla, CA 92093, USA E-mail: fweber@sdsu.edu

Abstract: We review the covariant density functional approach to the equation of state of the dense nuclear matter in compact stars. The main emphasis is on the hyperonization of the dense matter, and the role played by the Δ -resonances. The implications of hyperonization for the astrophysics of compact stars, including the equation of state, composition, and stellar parameters are examined. The mass-radius relation and tidal deformabilities of static and rapidly rotating (Keplerian) configurations are discussed in some detail. We briefly touch upon some other recent developments involving hyperonization in hot hypernuclear matter at high- and low-densities.

6

Keywords: Equation of state; Neutron stars; Gravitational waves

Contents

1.	I. Introduction							
2.	The Sample of Neutron Stars and its Mass Distribution							
	2.1. Types of mass measurements							
	2.2. Exploring the mass distribution of neutron stars	6						
3.	Maximum Mass of (Non-rotating, Isotropic) Neutron Stars							
	3.1. TOV equations for relativistic stellar structure	14						
	3.2. The Rhoades-Ruffini limit of a neutron star mass	16						
	3.3. Redback/black widow binary systems and the maximum mass/lightest							
	black hole problem	23						
	3.4. GW detection events and the possibility of NS masses above $\sim 2.5~M_{\odot}$.	26						
4.	Gravitational Waves from Merging NS							
	4.1. Inferring the Masses of NS from GW Events	28						
	4.2. Asymmetry in the systems GW170817 and GW190425	29						
5.	Neutron Star Birth Events	32						
	5.1. Neutron stars formed in single explosions	33						
	5.2. Neutron stars formed in binaries	39						
	5.3. The Accretion-Induced Collapse channel for NS formation	4(
6.	Conclusions	4						
Bil	pliography	45						

1. Introduction

Compact (or neutron) stars represent the endpoints of the evolution of ordinary stars. They provide a natural astrophysical laboratory for particle and nuclear physics under conditions that are largely different from and often inaccessible in terrestrial laboratories. For example, densities reached in compact stars are by a factor 5-10 larger than found in ordinary nuclei. In the 60s and 70s of the past century it has been conjectured that they may contain non-nucleonic constituents of matter, for example, hyperons (Ambartsumyan and Saakyan, 1960, 1961; Leung and Wang, 1971; Moszkowski, 1974; Pandharipande, 1971) or deconfined quark matter (Collins and Perry, 1975; Itoh, 1970). The state of (hyper)nuclear matter found in compact stars may feature some extraordinary facets, such as superfluidity and superconductivity, a trapped neutrino component at the early stages of evolution, and super-strong magnetic fields, for reviews see Glendenning (2012); Oertel et al. (2017); Sedrakian (2007); Shapiro and Teukolsky (1983); Weber (1999).

One of the key theoretical challenges of the description of compact stars is the diversity of the possible phases at high densities. A compact star has a (conservatively estimated) mass in the range $1.1 \lesssim M/M_{\odot} \lesssim 2.3$,

(1999).

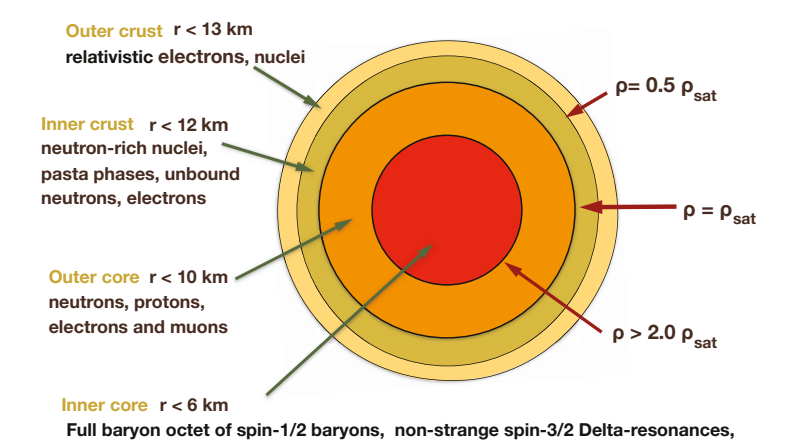


Fig. 1. Schematic illustration of the interior of a $M=1.4M_{\odot}$ mass neutron star. The transition density between different regions (in units of nuclear saturation density $\rho_{\rm sat}$) and the corresponding radial coordinate are indicated. The particle content of each

mesonic Bose condensates, color superconducting phases of dense quark matter

quark matter and hypernuclear matter. where M_{\odot} is the solar mass, the central densities may reach up to about 10 times the nuclear saturation density ($\rho_{\rm sat}=0.16~{\rm fm^{-3}}$), and a radius in the range $12\lesssim R\lesssim 14~{\rm km}$. A compact star consists roughly of five major regions: the atmosphere, the outer and inner crust, and the outer and inner core, see Fig. 1. The outer and inner crusts are characterized by

region are indicated as well. Note the possibility of mixed phases involving deconfined

the presence of the nuclear clusters immersed in electron gas and a neutron sea in the inner crust. The outer core consists of neutrons, protons, and leptons (mainly electrons with some admixture of muons). The composition of the inner core starting at about twice the nuclear saturation density is not well established: the multitude of possibilities include hyperonization, the deconfinement phase transition to quark matter, the onset of meson condensation, etc. For a textbook discussion of the phases of compact stars see, for example Glendenning (2012); Shapiro and Teukolsky (1983); Weber

During the last decade, there have been several breakthrough observational advances that reshaped our understanding of compact stars. These include the measurements of heavy pulsar masses in binaries of neutron stars with white dwarfs, the observation of gravitational waves from double neutron stars mergers, and the simultaneous mass and radius measurement of nearby X-ray emitting neutron stars. These advances provided crucial insights for the development of theoretical models of dense matter in recent years. Most importantly, they allowed us to narrow down substantially the theoretical range of parameters of the models of dense matter.

This review aims to present recent advances in the studies of the equation of state, composition, and physical manifestations of compact stars that contain hypernuclear cores. This will be done in the framework of the covariant density functional (hereafter CDF) methods (Serot and Walecka, 1997) for the description of dense hypernuclear matter - a method that provides a flexible enough approach to accommodate the information coming from astrophysics and laboratory on hypernuclei. The Lagrangian-based relativistic CDFs of nuclear systems (also known as nuclear relativistic mean-field models) operate with effective degrees of freedom - baryons and meson. They provide a well-motivated and straightforward way to obtain the energy density of matter. At the same time, there is no true fundamental field theory (in the sense of electroweak theory or QCD) associated with these models, i.e., the microscopic underpinning of these models is unknown. Therefore, they are best viewed as CDFs with parameters to be determined from available data in the sense of Kohn-Sham density functional theories which have been successfully applied in many complex many-body systems in various fields, including strongly correlated electronic systems, quantum chemistry, atomic and molecular systems, etc. The relativistic mean-field model based CDFs have been applied to hypernuclear systems already in 80s and 90s (Glendenning, 1985; Glendenning and Moszkowski, 1991; Glendenning et al., 1992; Huber et al., 1994, 1998; Papazoglou et al., 1998; Schaffner and Mishustin, 1996).

The motivation to study hypernuclear stars and the interest in hypernuclear CDFs resurged after the observations of two solar mass pulsars in a binary orbit with a white dwarf in 2010 (Demorest et~al., 2010) when, for the first time since the discovery of a pulsar in 1967, radioastronomy provided us with a significant constraint on the mass of a pulsar. The reason is that hyperons become energetically favorable once the Fermi energy of neutrons exceeds their rest mass. The onset of hyperons reduces the degeneracy pressure of a cold hypernuclear matter, therefore, its equation of state (hereafter EoS) becomes softer than that of nucleonic matter. As a result, the maximum possible mass of a compact star with hyperons decreases to values below $2M_{\odot}$ (Baldo et~al., 2000; Schulze and Rijken, 2011),

which is in direct contradiction with the observations. This contradiction is known as the "hyperon (or hyperonization) puzzle". As discussed below the modern density functionals for the hypernuclear matter not only resolve the hyperon puzzle but also account for the data coming from gravitational wave physics and X-ray observations of nearby pulsars (Banik et al., 2014; Bednarek et al., 2012; Bonanno and Sedrakian, 2012; Colucci and Sedrakian, 2013; Drago et al., 2016; Fortin et al., 2017, 2020; Gomes et al., 2019, 2015; Gusakov et al., 2014; Jiang et al., 2012; Li et al., 2018a,b; Lopes and Menezes, 2014; Maslov et al., 2015; Maslov et al., 2016; Massot et al., 2012; Miyatsu et al., 2015; Oertel et al., 2016, 2015; Providencia and Rabhi, 2013; Tolos et al., 2016; Torres et al., 2017; Tsubakihara and Ohnishi, 2013; van Dalen et al., 2014; Weissenborn et al., 2012a). The possibility of nucleation of Δ -resonances has been considered along with the hyperonization based on essentially the same arguments which make heavy baryons preferable to highly energetic neutrons (Choudhury and Rakshit. 1993; Sawyer, 1972; Schürhoff et al., 2010; Waldhauser et al., 1987, 1988; Weber and Weigel, 1989b). Again, after the discovery of massive pulsars, the CDF methods have been invoked to treat Δ -resonance admixed (hyper)nuclear matter (Cai et al., 2015; Dexheimer et al., 2021b; Drago et al., 2014; Kolomeitsev et al., 2017; Li et al., 2018b; Raduta et al., 2020; Ribes et al., 2019; Sahoo et al., 2018; Spinella and Weber, 2020; Thapa et al., 2020, 2021; Zhu et al., 2016).

Because of space limitations, we will focus in this review on the CDF approach and do not cover the alternative many-body approaches as applied to hypernuclei and compact stars, which include lattice studies (Inoue and HAL QCD Collaboration, 2019; Nemura et al., 2007; Sasaki et al., 2020), many-body schemes based on G-matrix theory (Bombaci, 2017; Haidenbauer et al., 2017; Yamamoto et al., 2014), Monte-Carlo (Gandolfi and Lonardoni, 2017; Lonardoni et al., 2013a, 2015, 2013b) and variational (Shahrbaf et al., 2020; Shahrbaf and Moshfegh, 2019; Togashi et al., 2016) methods, see also the reviews (Blaschke and Chamel, 2018; Chatterjee and Vidaña, 2016; Providência et al., 2019; Vidaña, 2018). An overview of the many-body methods with an emphasis on the compact stars can be found, for example, in Oertel et al. (2017); Sedrakian (2007).

Compact star properties will be discussed below exclusively with Einstein's theory of general relativity. However, there has been substantial work in recent years on the interpretation of the astrophysics of compact stars within alternative theories of gravity, see, for example Altaha Motahar et al. (2017); Astashenok et al. (2014, 2015a,b); Blázquez-Salcedo et al.

(2016) and references therein.

This chapter is organized as follows. Section 2 discusses the astrophysical constraints on compact star properties that became available in recent years. The key ideas of the CDF theory are presented in Sec. 3. Section 4 is devoted to the properties of hypernuclear stars, including the equation of state, composition, and global properties. The recent results on rapidly rotating hypernuclear stars are discussed in Sec. 5. The interplay between clustering and heavy-baryon degrees of freedom in the warm and low-density nuclear matter is exposed in Sec. 6. The cooling of hypernuclear stars, the finite-temperature equation of state, and universal relations are briefly touched upon in Sections 7 and 8, which is followed by concluding remarks in Sec. 9.

2. Astrophysical Constraints on Neutron Stars

Pulsar timing is among the methods that provide information on the masses of pulsars via measurements of the Keplerian parameters and the observed spin properties of pulsars within neutron star-neutron star and neutron star-white dwarf binaries. The Shapiro delay method of measurement of pulsar mass is based on the observation that electromagnetic radiation experiences a time delay as it passes in the vicinity companion compact object (neutron star or white dwarf) due to its gravitational field. The Shapiro delay method (Shapiro, 1964) has been successfully applied in binary systems involving millisecond pulsars, where the periodic pulsed signal from the pulsar covers tracks of different length within the space-time continuum depending on whether the pulsar passes in front or behind its binary companion relative to a distant observer. In the general theory of relativity, the Shapiro time delay depends on the companion mass and the degree of inclination of the binary system. The first high-mass pulsar measurement was carried out for PSR J1614-2230 which is a 3.2-ms pulsar in an 8.7-day orbit with a massive white-dwarf companion in a highly inclined orbit (Demorest et al., 2010). The second massive pulsar with high-precision mass measurement is J0348+0432 which is 39 ms pulsar in a 2.46-hour orbit with a white dwarf. In this case, optical observation and modeling of companion white dwarf was used in addition to pulsar timing measurements of Keplerian parameters of binary to place the mass of this millisecond pulsar at $2.01 \pm 0.04 M_{\odot}$ (Antoniadis et al., 2013). Improved measurements by the NANOGrav place the mass of this pulsar as $1.928(17)M_{\odot}$ (Fonseca et al., 2016). The third, most massive (measured with high-precision) neutron star to date is PSR J0740+6620 (Cromartie et~al., 2020), which is a 2.89-ms pulsar in a 4.77-day orbit with a white dwarf. The timing analysis which measures Shapiro delay places the mass of this pulsar at $2.08 \pm 0.07 M_{\odot}$ at 68.3% credibility (Fonseca et~al., 2021). Thus, the timing observations of three millisecond pulsars J1614-2230, J0348+0432, and J0740+6620 indicate that compact stars with masses as large as $2M_{\odot}$ exist in Nature. On the other hand, general relativity predicts that stable compact star sequences end at a maximal mass independent of the equation of state employed. (The stable configurations are determined by the Bardeen-Thorne-Meltzer criterion (Bardeen et~al., 1966), which implies that a star is stable only as long as its mass is increasing with the central density). Therefore, we may conclude that this maximum mass predicted by any viable EoS must be at least as large as those observed in the timing observations. In other words, the millisecond pulsar observations place a lower limit on the maximum mass of a compact star.

With the advent of gravitational wave astronomy and the first measurement by the LIGO and Virgo collaboration (hereafter LVC) of the gravitational waves from a binary neutron star (hereafter BNS) merger in the GW170817 event (Abbott et al., 2017) it became possible to constrain the properties of compact stars through the study of their tidal response. A weaker signal was detected later in the GW190425 event, which is likely to be a BNS coalescence (Abbott, 2020). These measurements, which were carried by the LVC second-generation ground-based gravitational observatories, are based on the idea that a neutron star is deformed in the tidal gravitational field of the companion. To the lowest order, such deformations are described through the star's induced quadrupole moment. The gravitational wave signal emitted before the merger of a binary carries direct information on the tidal properties of compact stars. The tidal deformability λ is defined as the coefficient which relates the induced quadrupole Q_{ij} to the perturbing tidal field \mathcal{E}_{ij} that acts on a star perturbing its shape $Q_{ij} = -\lambda \mathcal{E}_{ij}$, where i and j label the space coordinates. It is related to the gravitational Love number k_2 via the relation

$$\lambda = \frac{2}{3}k_2R^5,\tag{1}$$

which exhibits its sensitivity to the radius of the star R. Both k_2 and R depend on the EoS of matter (Baiotti, 2019). Frequently one uses dimensionless tidal deformability defined as

$$\Lambda = \frac{\lambda}{M^5} = \frac{2}{3}k_2C,\tag{2}$$

where C = M/R is the compactness of the star. Frequently one also defines an effective tidal deformability as (Flanagan and Hinderer, 2008)

$$\tilde{\Lambda} = \frac{16}{13} \frac{(M_1 + 12M_2)M_1^4 \Lambda_1 + (M_2 + 12M_1)M_2^4 \Lambda_2}{(M_1 + M_2)^5},$$
(3)

involving the masses and tidal deformabilities of both stars. The analysis of the GW170817 and GW190425 events were carried out for high- and low-spin priors. We give below some characteristic numbers only for low-spin priors as suggested by galactic observations. The total binary mass values $2.73^{+0.04}_{-0.01} M_{\odot}$ and $3.4^{+0.3}_{-0.1} M_{\odot}$ were deduced from the GW170817 and GW190425 events. The masses of the components are in the range $1.16-1.6 M_{\odot}$ for GW170817 and $1.46-1.87 M_{\odot}$ for GW190425 event. The analysis of GW170817 event led to an upper limit $\Lambda_{1.4} < 700$ for a $1.4 M_{\odot}$ star (90% confidence). In the case of the GW190425 event, $\tilde{\Lambda} \leq 600$ has been inferred for the binary mass range indicated above.

Neutron star surfaces are emitting X-rays due to their thermal heating by currents associated with the particle flows in the magnetosphere. The location of the emitting hot spots reflects the structure and topology of the magnetosphere. Due to the rotation of the star, the hot spots are generating pulsed emission. The thermal X-ray emission pulse profile of millisecond pulsar J0030+0451 has been used by the NICER team to place limits on its mass and radius (Miller et al., 2019; Riley et al., 2019). The procedure involves modeling the soft X-ray pulses produced by the rotation of hot spots on the surface of the star and fitting them to the NICER waveform data. In doing so it was assumed that the star's emitting atmosphere is ionized hydrogen and that the magnetic field does not play any role. The two independent analyses predict (68% credible interval) $M=1.44^{+0.15}_{-0.14}M_{\odot},~R=13.02^{+1.24}_{-1.06}~{\rm km}$ (Miller *et al.*, 2019) and $M=1.34^{+0.15}_{-0.16}M_{\odot},~R=12.71^{+1.14}_{-1.19}~{\rm km}$ (Riley *et al.*, 2019). The same collaboration has also measured the radius of PSR J0740+662 to be $R = 13.7^{+2.6}_{-1.5}$ km (Miller et al., 2021) and $R = 12.39^{+1.3}_{-0.98}$ km (Riley et al., 2021) (68% credible interval). In addition to the above constraints, the masses of neutron stars in binaries have been measured with high accuracy which lie in the range $1.2 \lesssim M/M_{\odot} \lesssim 1.6$ with a significant concentration around the value 1.4 M_{\odot} (Lattimer, 2019; Özel and Freire, 2016). Furthermore, the moment of inertia of a neutron star is expected to be measured in the double pulsar system PSR J0737-3039 (Lattimer and Schutz, 2005), where both masses of stars are already accurately determined by observations.

3. Density Functionals for Hypernuclear Matter

Density functional theory offers a flexible framework to study the equilibrium thermodynamics of nuclear and neutron star matter. In nuclear physics, a particular class of density functionals can be obtained within the so-called "relativistic mean-field" models of nuclear matter, which by construction posses the main feature of density functional theory: the potential energy of the zero-temperature system is a functional of (energy) density alone. The self-energies in these theories are evaluated either in the Hartree or Hartree-Fock theories of many-body theory, the first approximation being the simplest realization of such scheme. The Hartree-Fock theories allow one to introduce the pion contribution explicitly in the density functional, which could be an advantage for a detailed treatment of the tensor force. Once the density functional is constructed the parameters of the relativistic Lagrangian are adjusted to reproduce the laboratory data within a range that is compatible with other constraints, such as those available from compact star observations. The microscopic ab initio many-body calculations are treated as data, i.e., they constrain the admissible range of parameters entering the functional. (In passing we note that density functionals have been derived directly from microscopic theories, but this will not be reviewed here). An advantage of the approach taken here is the straightforward extension of the density functional from nuclear to hypernuclear and Δ -resonance matter. The fast numerical implementations allow us to scan a large parameter space associated with the density functional, which can become quite large as one includes the heavy baryons in the functional.

3.1. Relativistic density functional with density-dependent couplings

In this section, we briefly review the construction of the density functional of hypernuclear matter starting from a relativistic Lagrangian and adopting the Hartree approximation. The Hartree-Fock scheme is discussed in detail elsewhere (Li et al., 2018a). We will use a particular class of such functionals that assign a density dependence to the coupling constants describing the meson-baryon interactions, which incorporate modifications of the interaction due to changes in the density of the medium in which baryons and mesons are embedded (Lalazissis et al., 2005; Typel, 2018; Typel and Wolter, 1999). The scheme discussed below will include successively the J=1/2 baryon octet and J=3/2 resonances; see Fig. 2 for an illustra-

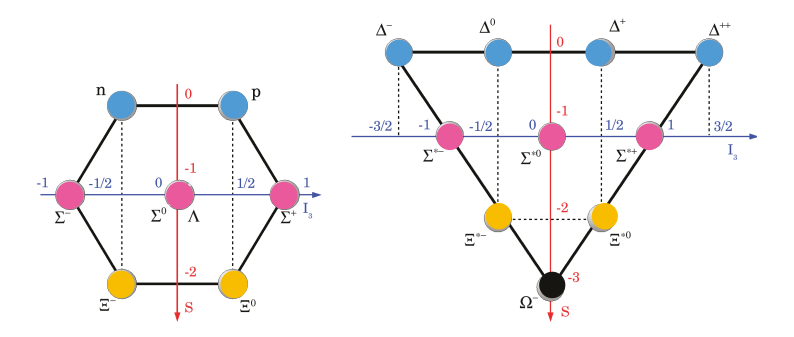


Fig. 2. An illustration of the spin-1/2 octet of baryons (left) and spin-3/2 decuplet of resonances (right), where the vertical axis is the strangeness and the horizontal axis is the third component of the isospin.

tion of the octet and decuplet arrangement of the heavy baryons and their quantum numbers. The Lagrangian of stellar matter with baryonic degrees of freedom can be written as

$$\mathcal{L} = \mathcal{L}_b + \mathcal{L}_m + \mathcal{L}_l + \mathcal{L}_{em}, \tag{4}$$

where the baryon Lagrangian is given by

$$\mathcal{L}_{b} = \sum_{b} \bar{\psi}_{b} \left[\gamma^{\mu} \left(i \partial_{\mu} - g_{\omega b} \omega_{\mu} - \frac{1}{2} g_{\rho B} \tau \cdot \rho_{\mu} \right) - (m_{b} - g_{\sigma b} \sigma) \right] \psi_{b}, \quad (5)$$

where the b-sum is over the $J^P = \frac{1}{2}^+$ baryon octet, ψ_b are the baryonic Dirac fields of baryons with masses m_b , and σ , ω_μ , and ρ_μ are the mesonic fields which mediate the interaction among baryon fields. The coupling constants g_{mb} , in general, are density-dependent. The mesonic part of the Lagrangian is given by

$$\mathscr{L}_{m} = \frac{1}{2} \partial^{\mu} \sigma \partial_{\mu} \sigma - \frac{m_{\sigma}^{2}}{2} \sigma^{2} - \frac{1}{4} \omega^{\mu\nu} \omega_{\mu\nu} + \frac{m_{\omega}^{2}}{2} \omega^{\mu} \omega_{\mu} - \frac{1}{4} \rho^{\mu\nu} \cdot \rho_{\mu\nu} + \frac{m_{\rho}^{2}}{2} \rho^{\mu} \cdot \rho_{\mu},$$

$$(6)$$

where m_{σ} , m_{ω} , and m_{ρ} are the meson masses and $\omega_{\mu\nu}$ and $\rho_{\mu\nu}$ represent the strength tensors of vector mesons

$$\omega_{\mu\nu} = \partial_{\mu}\omega_{\nu} - \partial_{\mu}\omega_{\nu}, \qquad \boldsymbol{\rho}_{\mu\nu} = \partial_{\nu}\boldsymbol{\rho}_{\mu} - \partial_{\mu}\boldsymbol{\rho}_{\nu}. \tag{7}$$

The leptonic Lagrangian is given by

$$\mathcal{L}_{l} = \sum_{\lambda} \bar{\psi}_{\lambda} (i\gamma^{\mu}\partial_{\mu} - m_{\lambda})\psi_{\lambda}, \tag{8}$$

where ψ_{λ} are lepton fields (in stellar matter the λ -summation includes electron, muons, and at high temperatures the three flavors of neutrinos when neutrinos are trapped) and m_{λ} are their masses. Finally, if the stellar matter is permeated by sizable magnetic fields (which is the case, for example, in magnetars) then we need to include the electromagnetism via its gauge-field Lagrangian

$$\mathcal{L}_{\rm em} = -\frac{1}{4} F^{\mu\nu} F_{\mu\nu},\tag{9}$$

where $F^{\mu\nu}$ is the electromagnetic field strength tensor and replace the partial derivatives by their gauge-invariant counterparts $D_{\mu} = \partial_{\mu} + ieQA_{\mu}$ where A_{μ} is the electromagnetic vector potential and eQ is the charge of the particle (Dexheimer et~al., 2021b; Thapa et~al., 2020).

The baryonic Lagrangian can be extended to include the non-strange J=3/2 members of the baryons decuplet which is the quartet of Δ -resonances, see Fig. 2, by adding to the Lagrangian (4) the term

$$\mathcal{L}_{d} = \sum_{d} \bar{\psi}_{d}^{\nu} \left[\gamma^{\mu} \left(i \partial_{\mu} - g_{\omega d} \omega_{\mu} - \frac{1}{2} g_{\rho d} \tau \cdot \rho_{\mu} \right) - (m_{d} - g_{\sigma d} \sigma) \right] \psi_{d\nu}, (10)$$

where the d-summation is over the resonances described by the Rarita-Schwinger fields $\psi_{d\nu}$. Furthermore, to describe the interactions between the strange particles the Lagrangian (4) can be extended to include the interactions in the hypernuclear sector via two additional (hidden strangeness) mesons σ^* and ϕ

$$\mathcal{L}_{m'} = \frac{1}{2} \partial^{\mu} \sigma^* \partial_{\mu} \sigma^* - \frac{m_{\sigma}^{*2}}{2} \sigma^{*2} - \frac{1}{4} \phi_{\mu\nu} \phi^{\mu\nu} + \frac{1}{2} m_{\phi}^2 \phi_{\mu} \phi^{\mu}, \tag{11}$$

with field strength tensor $\phi_{\mu\nu} = \partial_{\nu}\phi_{\mu} - \partial_{\mu}\phi_{\nu}$. These mesons do not couple to nucleons, i.e., $g_{\sigma^*N} = g_{\phi N} = 0$, see however Eq. (29) below.

Let us now turn to the coupling constants in the nucleonic sector. These are given by their values at the saturation density $\rho_{\rm sat}$ and by functional form describing their dependence on baryon density ρ_B

$$g_{iN}(\rho_B) = g_{iN}(\rho_{\text{sat}})h_i(x), \tag{12}$$

where $x = \rho_B/\rho_{\rm sat}$ and

$$h_i(x) = \frac{a_i + b_i(x + d_i)^2}{a_i + c_i(x + d_i)^2}, \ i = \sigma, \omega, \quad h_\rho(x) = e^{-a_\rho(x - 1)}.$$
 (13)

The density dependence of the couplings implicitly takes into account many-body correlations that modify the interactions in the medium. In the following we will adopt the DDME2 parametrization (Lalazissis *et al.*, 2005); the values of the parameters are listed for completeness in Table 1.

Table 1. The values of parameters of the DDME2 CDF.

Meson (i)	$m_i \; (\mathrm{MeV})$	a_i	b_i	c_i	d_i	g_{iN}
σ	550.1238	1.3881	1.0943	1.7057	0.4421	10.5396
ω	783	1.3892	0.9240	1.4620	0.4775	13.0189
ρ	763	0.5647				7.3672

The masses of ω and ρ mesons are taken to be their free values. The five constraints $h_i(1) = 1$, $h_i''(0) = 0$ and $h_{\sigma}''(1) = h_{\omega}''(1)$ allow one to reduce the number of free parameters in isocalar-scalar and iso-scalar-vector sector to three. Three additional parameters in this channel are $g_{\sigma N}(\rho_{\rm sat}), g_{\omega N}(\rho_{\rm sat})$ and m_{σ} - the mass of the phenomenological σ meson. With two additional parameter in the isovector-vector channel, the parameterization has in total eight parameters (seven entering the definition of the coupling constants and the mass of the σ -meson) which are adjusted to reproduce the properties of symmetric and asymmetric nuclear matter, binding energies, charge radii, and neutron skins of spherical nuclei.

The ground-state expectation values of mesons in the mean-field and infinite system approximations are given by

$$m_{\sigma}^{2}\sigma = \sum_{b} g_{\sigma b} n_{b}^{s} + \sum_{d} g_{\sigma d} n_{d}^{s}, \quad m_{\sigma^{*}}^{2}\sigma^{*} = \sum_{b} g_{\sigma^{*}b} n_{b}^{s},$$
 (14)

$$m_{\sigma}^{2} \sigma = \sum_{b} g_{\sigma b} n_{b}^{s} + \sum_{d} g_{\sigma d} n_{d}^{s}, \quad m_{\sigma^{*}}^{2} \sigma^{*} = \sum_{b} g_{\sigma^{*} b} n_{b}^{s},$$
(14)
$$m_{\omega}^{2} \omega_{0} = \sum_{b} g_{\omega b} n_{b} + \sum_{d} g_{\omega d} n_{d}, \quad m_{\phi}^{2} \phi_{0} = \sum_{b} g_{\phi b} n_{b},$$
(15)

$$m_{\rho}^{2}\rho_{03} = \sum_{b} g_{\rho b} \boldsymbol{\tau}_{b3} n_{b} + \sum_{d} g_{\rho d} \boldsymbol{\tau}_{d3} n_{d},$$
 (16)

where the scalar and baryon (vector) number densities are defined for the baryon octet as $n_b^s = \langle \bar{\psi}_b \psi_b \rangle$ and $n_b = \langle \bar{\psi}_b \gamma^0 \psi_b \rangle$, respectively. For the Δ -resonances, these are defined as $n_d^s = \langle \bar{\psi}_{d\nu} \psi_d^{\nu} \rangle$ and $n_d = \langle \bar{\psi}_{d\nu} \gamma^0 \psi_d^{\nu} \rangle$, respectively. The effective (Dirac) baryon masses in the same approximation are given by

$$m_b^* = m_b - g_{\sigma b}\sigma - g_{\sigma^* b}\sigma^*, \quad m_d^* = m_d - g_{\sigma d}\sigma. \tag{17}$$

Given the Lagrangian density (5), the energy stress tensor can be constructed

$$T^{\mu\nu} = \frac{\partial \mathcal{L}}{\partial(\partial_{\mu}\varphi_{i})} \partial^{\nu}\varphi_{i} - g^{\mu\nu}\mathcal{L}, \tag{18}$$

where φ_i stands generically for a boson or fermion field. Then, its diagonal elements define the energy density and pressure

$$\mathcal{E} = \langle T^{00} \rangle, \quad P = \frac{1}{3} \sum_{i} \langle T^{ii} \rangle,$$
 (19)

where the brackets refer to statistical averaging. Explicitly one finds

$$P = -\frac{m_{\sigma}^{2}}{2}\sigma^{2} - \frac{m_{\sigma}^{*2}}{2}\sigma^{*2} + \frac{m_{\omega}^{2}}{2}\omega_{0}^{2} + \frac{m_{\rho}^{2}}{2}\rho_{03}^{2} + \frac{m_{\phi}^{2}}{2}\phi_{0}^{2} + \frac{1}{3}\sum_{b,d}\frac{2J_{b,d}+1}{2\pi^{2}}\int_{0}^{\infty}\frac{dk}{E_{k}^{b,d}}\left[f(E_{k}^{b,d}-\mu_{b,d}^{*})+f(E_{k}^{b,d}+\mu_{b,d}^{*})\right] + \frac{1}{3\pi^{2}}\sum_{\lambda}\int_{0}^{\infty}\frac{dk}{E_{k}^{\lambda}}\left[f(E_{k}^{\lambda}-\mu_{\lambda})+f(E_{k}^{\lambda}+\mu_{\lambda})\right],$$
 (20)

and

$$\mathcal{E} = \frac{m_{\sigma}^{2}}{2}\sigma^{2} + \frac{m_{\sigma}^{*2}}{2}\sigma^{*2} + \frac{m_{\omega}^{2}}{2}\omega_{0}^{2} + \frac{m_{\rho}^{2}}{2}\rho_{03}^{2} + \frac{m_{\phi}^{2}}{2}\phi_{0}^{2} + \sum_{b,d} \frac{2J_{b,d} + 1}{2\pi^{2}} \int_{0}^{\infty} dk \ k^{2}E_{k}^{b,d} \left[f(E_{k}^{b,d} - \mu_{b,d}^{*}) + f(E_{k}^{b,d} + \mu_{b,d}^{*}) \right] + \sum_{\lambda} \int_{0}^{\infty} \frac{dk}{\pi^{2}} k^{2}E_{k}^{\lambda} \left[f(E_{k}^{\lambda} - \mu_{\lambda}) + f(E_{k}^{\lambda} + \mu_{\lambda}) \right],$$
 (21)

where J_B is the baryon degeneracy factor,

$$\mu_b = \sqrt{p_{F_b}^2 + m_b^{*2}} + g_{\omega b}\omega_0 + g_{\phi b}\phi_0 + g_{\rho b}\tau_{b3}\rho_{03} + \Sigma^r,$$
 (22)

$$\mu_d = \sqrt{p_{F_d}^2 + m_d^{*2}} + g_{\omega d}\omega_0 + g_{\rho d}\tau_{d3}\rho_{03} + \Sigma^r, \tag{23}$$

are the baryon chemical potentials, I_3 is the third component of baryon isospin, $E_k^{b,d} = \sqrt{k^2 + m_{b,d}^{*2}}$ and $E_k^{\lambda} = \sqrt{k^2 + m_{\lambda}^2}$ are the single particle energies of baryons and leptons respectively, and $f(E) = [1 + \exp(E/T)]^{-1}$ is the Fermi distribution function at temperature T. The lepton mass m_{λ} can be taken equal to its free-space value. The self-energy Σ^r arises due to the density-dependence of the coupling constant and guarantees the thermodynamic consistency of the theory, i.e., the fact that the thermodynamic relation

$$P = \rho^2 \frac{\partial}{\partial \rho} \left(\frac{\mathcal{E}}{\rho} \right) \,, \tag{24}$$

is fulfilled.

3.2. Hyperonic and Δ -resonance couplings

The lack of reliable information on the hyperon-nucleon and hyperonhyperon interactions prevents a high-precision determination of the parameters entering the Lagrangian (5). The SU(3) flavor symmetric model allows one to determine the magnitude of the coupling constants appearing in the Lagrangian (5) based on symmetry argument and the principles of the "eightfold way" of elementary particle classification in particle physics (de Swart, 1963). The SU(3) symmetry in flavor space is, of course, broken by the strange quark mass at the densities and temperatures relevant to compact stars. Nevertheless, it provides some guidance in instances where no or little information is available.

Within this model, the spin-1/2 baryons and mesons are arranged in octets, which is the lowest non-trivial irreducible representation of the symmetry group. The interaction part of the SU(3) invariant Lagrangian describing the coupling of baryons and mesons is constructed using matrix representations for the baryon $J^P = 1/2^+$ octet of baryons B and $J^P = 1^-$ meson octet (M_8) which is supplemented by meson singlet (M_1) which allows describing physical mesons via mixing mechanism. The Lagrangian contains linear combinations of the antisymmetric (F-type), symmetric (D-type), and singlet (S-type) scalar contributions (using the standard notations)

$$\mathcal{L}_{SU(3)} = -g_8\sqrt{2}[\alpha \text{Tr}([\bar{B}, M_8]B) + (1 - \alpha)\text{Tr}(\{\bar{B}, M_8\}B)]$$
$$-\frac{g_1}{\sqrt{3}}\text{Tr}(\bar{B}B)\text{Tr}(M_1), \tag{25}$$

where g_8 and g_1 denote the meson octet and singlet coupling constant respectively and $\alpha = F/(F+D)$ with $0 \le \alpha \le 1$.

The physical mesons ω and ϕ then appear as a mixture of the ω_0 and ω_8 members of the vector meson nonet:

$$\begin{pmatrix} \omega_8 \\ \omega_0 \end{pmatrix} = \begin{pmatrix} \cos \theta_V & \sin \theta_V \\ -\sin \theta_V & \cos \theta_V \end{pmatrix} \begin{pmatrix} \omega \\ \phi \end{pmatrix} , \tag{26}$$

where θ_V is the vector mixing angle. Within this mixing scheme the coupling of a baryon to the physical ω -meson is given by

$$g_{B\omega} = \cos \theta_V g_1 + \sin \theta_V \frac{g_8}{\sqrt{3}} \delta_B, \qquad B \in \{N, \Xi, \Lambda, \Sigma\},$$
 (27)

where $\delta_N = 4\alpha_V - 1$, $\delta_{\Xi} = 1 + 2\alpha_V$ and $\delta_{\Sigma} = -\delta_{\Lambda} = 2(1 - \alpha_V)$. It is convenient to express the coupling of hyperons to mesons by using the nucleonic couplings as normalization

$$R_{\omega B} = \frac{g_{\omega B}}{g_{\omega N}} = \frac{1 - \frac{g_8}{g_1\sqrt{3}}\delta_B \tan\theta_V}{1 - \frac{g_8}{g_1\sqrt{3}}(1 - 4\alpha_V)\tan\theta_V}.$$
 (28)

The ϕ -meson couplings can be obtained from those for ω meson by the substitution $\cos \theta_V \to -\sin \theta_V$ and $\sin \theta_V \to \cos \theta_V$. In general, it is possible that ϕ meson couples to the nucleon with the coupling given by

$$R_{\phi N} = -\frac{\tan \theta_V - \frac{g_8}{g_1 \sqrt{3}} \delta_N}{1 + \frac{g_8}{g_1 \sqrt{3}} \delta_N \tan \theta_V}.$$
 (29)

The coupling for the isovector ρ meson is given by

$$g_{\rho N} = g_8, \quad R_{\rho \Xi} = -(1 - 2\alpha_V), \quad R_{\rho \Sigma} = 2\alpha_V, \quad R_{\rho \Lambda} = 0.$$
 (30)

Note that the ρ couplings vanish exponentially at high densities according to Eq. (13) and their effect on the properties of dense matter (beyond the threshold for the onset of hyperons) is small.

The approximate equality of the masses of ω and ρ -mesons implies that the mixing is ideal, in which case ϕ meson is a pure $\bar{s}s$ state and the mixing angle is given by the *ideal mixing* value $\tan \theta_V^* = 1/\sqrt{2}$. Since the nucleon does not couple to pure strange meson ϕ , Eq. (29) implies that this is the case when $g_1 = \sqrt{6} g_8$ and $\alpha_V = 1$, the latter being the universality assumption for the (electric) F/(F+D) ratio, i.e., only F-type coupling is non-zero. In this case the coupling constants of heavy baryons are related to those of the nucleon as in the additive quark model.

The couplings in the case of the scalar mesons σ and σ^* , are obtained from those of ω and ϕ , respectively, with the replacements $\omega \to \sigma$, $\phi \to \sigma^*$, and changing the vector indices to scalar ones $V \to S$. In the case of σ -meson the coupling constants are given by

$$q_{B\sigma} = \cos \theta_S \ q_1 + \delta_B q_8 \sin \theta_S / \sqrt{3},\tag{31}$$

where in the definitions of δ_B the scalar ratio α_S appears instead of its vector counterpart. It can be shown that the coupling defined in this manner obey the following relation (Colucci and Sedrakian, 2013)

$$2(g_{N\sigma} + g_{\Xi\sigma}) = 3g_{\Lambda\sigma} + g_{\Sigma\sigma},\tag{32}$$

which is valid for arbitrary values of the four parameters α_S , g_1 , g_8 and θ_S . It is easy to verify that Eq. (32) is satisfied for the coupling constants in the SU(6) spin-flavor symmetric quark model. Table 2 lists the couplings within this model.

The information on the couplings of hyperons to the scalar mesons can be obtained from the fits to their potentials in nuclear matter and nuclei within a particular model. For example, the single Λ -hypernuclei has been used to fix the value of $g_{\Lambda\sigma}$ coupling (van Dalen *et al.*, 2014). Similarly,

Table 2. The ratios of the couplings of hyperons in the SU(6) spin-flavor model.

Y	$\backslash R$	$R_{\sigma Y}$	R_{σ^*Y}	$R_{\omega Y}$	$R_{\phi Y}$	$R_{\rho Y}$
1	1	2/3	$-\sqrt{2}/3$	2/3	$\sqrt{2}/3$	0
Σ	Ξ	2/3	$-\sqrt{2}/3$	2/3	$-\sqrt{2}/3$	2
Ξ	Ξ	1/3	$-2\sqrt{2}/3$	1/3	$-2\sqrt{2}/3$	1

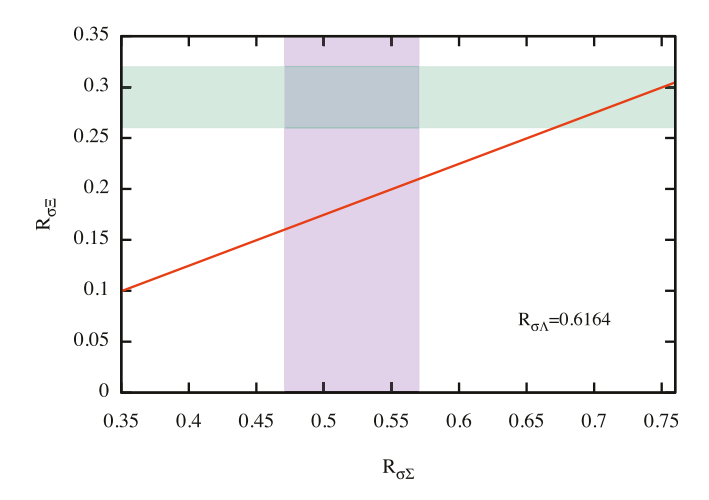


Fig. 3. The ranges of coupling constants $R_{\sigma\Sigma}$ and $R_{\sigma\Xi}$ (shaded areas) compatible with experimental/theoretical information and relation (32) (solid line) for DDME2 CDF and fixed $R_{\sigma\Lambda}=0.6164$. The combined area of $R_{\sigma\Sigma}$ and $R_{\sigma\Xi}$ has no overlap with prediction based on the SU(3) flavor symmetry, indicating its breaking in the scalar-meson sector.

the coupling to the σ^* is obtained from the fits to the binding of double Λ hypernuclei (Fortin *et al.*, 2017). Furthermore, density functionals have been adapted to treat multi-strange nuclei hypernuclei (Güven *et al.*, 2018; Khan *et al.*, 2015; Margueron *et al.*, 2017).

Figure 3 shows the range of the (dimensionless) couplings $R_{\sigma\Sigma}$ and $R_{\sigma\Xi}$ which covers the potential depths ranges $U_{\Sigma}(\rho_{\rm sat}) = [-10:+30]$ MeV and $U_{\Sigma}(\rho_{\rm sat}) = [-24:0]$ MeV at nuclear saturation density. The value $U_{\Xi}(\rho_{\rm sat}) = -24$ MeV has been given in (Friedman and Gal, 2021) and is much deeper than the one expected from Lattice 2019 results (Inoue and HAL QCD Collaboration, 2019; Sasaki *et al.*, 2020). The fixed value of the $R_{\sigma\Lambda} = 0.6164$ (van Dalen *et al.*, 2014) has been used. It is seen that in contrast to the SU(6) model, the values of $R_{\sigma\Xi}$ predicted by relation

(32) do not intercept the overlap area of $R_{\sigma\Sigma}$ and $R_{\sigma\Xi}$ couplings, which indicates the breaking of corresponding symmetry.

The results pertaining hyperonic compact stars below have been obtained with the parameters $R_{\sigma\Lambda}=0.6106,\ R_{\sigma\Sigma}=0.4426,\ {\rm and}\ R_{\sigma\Xi}=0.3024$ (Li et al., 2018b) in the framework of the DDME2 CDF extension to hypernuclear sector.

Most studies of Δs in dense matter have been carried out in the relativistic mean-field approach (Cai et al., 2015; Choudhury and Rakshit, 1993; Lavagno, 2010; Waldhauser et al., 1987, 1988; Weber and Weigel, 1989b), the density-dependent CDF approach (Drago et al., 2014; Kolomeitsev et al., 2017; Li et al., 2018b), the relativistic Hartree-Fock approach (Weber and Weigel, 1989a; Zhu et al., 2016) and the quark-meson coupling model (Motta et al., 2020). The interactions of Δ -resonance within the matter are not well known. Some information on the Δ -potential in the isospin symmetric nuclear matter is available from the analysis of scattering of electrons and pions off nuclei with Δ -excitation (Horikawa et al., 1980; Koch, 1997; Nakamura et al., 2010; O'Connell and Sealock, 1990; Wehrberger et al., 1989) and photo-absorption (Alberico et al., 1994; Riek et al., 2009). The extracted value of the potential is (Drago et al., 2014)

$$-30 \text{ MeV} + V_N(\rho_{\text{sat}}) \le V_\Delta(\rho_{\text{sat}}) \le V_N(\rho_{\text{sat}}), \tag{33}$$

where $V_N(\rho_{\rm sat})$ is the nucleon isoscalar potential at the saturation density. The Δ -resonance production in heavy-ion collisions is another channel of information, where however collective dynamics of nuclear matter comes into play (Cozma, 2016; Cozma and Tsang, 2021; Ono *et al.*, 2019; Xu, 2019). Numerical simulations provide hints towards the values of the potential in the range (Kolomeitsev *et al.*, 2017)

$$V_N(\rho_{\text{sat}}) \le V_\Delta(\rho_{\text{sat}}) \le 2/3V_N(\rho_{\text{sat}}).$$
 (34)

The isovector meson- Δ -resonance couplings are not known. In the following we use the ratios $R_{m\Delta} = g_{m\Delta}/g_{mN}$ to describe the Δ -resonance couplings. In the recent work, these parameters have been varied in the range (Li and Sedrakian, 2019a; Li *et al.*, 2018b)

$$R_{\rho\Delta} = 1, \quad 0.8 \le R_{\omega\Delta} \le 1.6, \quad R_{\sigma\Delta} = R_{\omega\Delta} \pm 0.2,$$
 (35)

to explore the consequences of the inclusion of Δ -resonance in the CDF of (hyper)nuclear matter.

Table 3. The coefficients of the expansion (36) for the DDME2 parametrization in MeV units, where we show the values of higher-order parameters not defined in (36), see Margueron *et al.* (2018a).

Density expansion								
$\rho_{\rm sat} [{\rm fm}^{-3}]$	m_N^*/m	$E_{\rm sat}$		K_{sat}	Q_{sat}	Z_{sat}		
0.152	0.57	-16.14		251.15	479	4448		
Isospin-asymmetry expansion								
		E_{sym}	L_{sym}	K_{sym}	Q_{sym}			
		32.31	51.27	-87	777			

3.3. Characteristics of nuclear matter close to saturation

As is well known, the EoS of nuclear matter can be parametrized via an expansion in the vicinity of saturation density and isospin-symmetrical limit via a double-expansion in the Taylor series:

$$E(\chi,\delta) \simeq E_{\text{sat}} + \frac{1}{2!} K_{\text{sat}} \chi^2 + \frac{1}{3!} Q_{\text{sat}} \chi^3 + E_{\text{sym}} \delta^2 + L_{\text{sym}} \delta^2 \chi + \mathcal{O}(\chi^4, \chi^2 \delta^2),$$
(36)

where $\chi = (\rho - \rho_{\rm sat})/3\rho_{\rm sat}$, $\delta = (\rho_n - \rho_p)/\rho$ with ρ_n and ρ_p being the neutron and proton densities. The coefficients of the expansion are known as incompressibility $K_{\rm sat}$, the skewness $Q_{\rm sat}$, the symmetry energy $E_{\rm sym}$ and the slope parameter $L_{\rm sym}$. The definitions of parameters are standard, see Margueron et al. (2018a). These four low-order coefficients can be constrained from experimental data on nuclear systems. The higher-order terms are less constrained (Margueron et al., 2018a; Zhang and Li, 2019).

While the CDFs provide full access to the spectra of particles, the matter compositions, etc. the expansions of the type (36) provide only a more limited set of physical parameters, for example, the EoS. Since the uncertainties in the nuclear matter properties are easily characterized in terms of uncertainties in the characteristics entering the expansion (36), it is important to establish a one-to-one correspondence between the two descriptions.

The five macroscopic characteristics in Eq. (36) together with the preassigned values of saturation density $\rho_{\rm sat}$ and the nucleon Dirac mass m_N^*/m uniquely determine the seven adjustable parameters of the CDFs of the DDME2 type. This allows one to generate new parametrizations which reproduce desired values of the characteristics (Li and Sedrakian, 2019a), especially those that are associated with high-density and large-isospin behavior. As finite nuclei do not probe these regimes the loss of accuracy of the new CDFs in reproducing the binding energies, charge radii and neutron skins of finite nuclei is marginal.

Having such a tool at the disposal one can now proceed to vary individually the characteristics within their acceptable ranges and extract the EoS of dense matter and, consequently, the properties of compact stars. This allows one to explore the correlation(s) between specific properties of nuclear matter and/or compact stars (Cai and Chen, 2017; Cai and Li, 2021; Li et al., 2021; Li and Magno, 2020; Li and Sedrakian, 2019a; Li and Sedrakian, 2019b). Detailed investigations of the EoS were carried out where the higher-order coefficients of the expansion, specifically, $Q_{\rm sat}$ and $L_{\rm sym}$ were varied since their values are weakly constrained by the conventional fitting protocol of CDF (Li and Sedrakian, 2019a; Margueron and Gulminelli, 2019; Margueron et al., 2018a,b; Zhang et al., 2018). It is interesting that the one-to-one mapping described above allows one to predict the higher-order terms in the expansion (36) (Li and Sedrakian, 2019a), which are highly model dependent (Dutra et al., 2014, 2012).

4. Hypernuclear Stars: static properties

4.1. EoS and composition

Given a CDF one could compute the EoS of the stellar matter by implementing the additional conditions of weak equilibrium and change neutrality that prevail in compact star matter (except for the first instances after birth). The strangeness changing weak equilibrium conditions are given

$$\mu_{\Lambda} = \mu_{\Sigma^0} = \mu_{\Xi^0} = \mu_{\Delta^0} = \mu_n = \mu_B,$$
(37)

$$\mu_{\Sigma^{-}} = \mu_{\Xi^{-}} = \mu_{\Delta^{-}} = \mu_{B} - \mu_{Q}, \tag{38}$$

$$\mu_{\Sigma^{+}} = \mu_{\Delta^{+}} = \mu_{B} + \mu_{Q},\tag{39}$$

$$\mu_{\Delta^{++}} = \mu_B + 2\mu_Q,\tag{40}$$

where μ_B and $\mu_Q = \mu_p - \mu_n$ are the baryon and charge chemical potentials, μ_i with $i \in \{\Lambda, \Sigma^{0,\pm}, \Xi^{0,\pm}, \Delta^{0,\pm,++}\}$ are the chemical potentials of the baryons. The baryonic charge is given by

$$n_p + n_{\Sigma^+} + 2n_{\Delta^{++}} + n_{\Delta^+} - (n_{\Sigma^-} + n_{\Xi^-} + n_{\Delta^-}) = n_Q,$$

where n_i are the baryon number densities. The electrical charge neutrality is then implemented by equating this quantity with the lepton charge

$$n_Q = n_e + n_\mu, \tag{41}$$

where $n_{e,\mu}$ are the number densities of electrons and muons. Figure 4 shows the EoS for nucleonic (N), hyperonic (NY) and Δ -admixed hyperonic $(NY\Delta)$ matter at zero temperature and in weak β -equilibrium. The

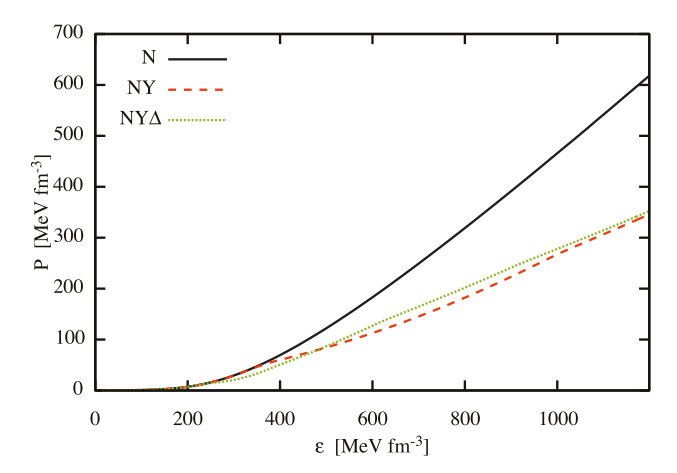


Fig. 4. The EoS of nucleonic (N), hyperonic (NY) and Δ -admixed hyperonic $(NY\Delta)$ matter at zero temperature and in β -equilibrium. The Δ -potential is fixed by $V_{\Delta}(\rho_{\text{sat}}) = V_N(\rho_{\text{sat}})$.

onset of hyperons and Δ particles are seen by the change in the slope of the pressure above the saturation density and significant softening of the EoS. In the case where Δ 's are included in the composition, the EoS softens at low and stiffens at high densities compared to the purely hyperonic case. Figure 5 shows the particle abundances of hyperonic matter for the DDME2 plus hyperons parameterization. This EoS is smoothly matched at the density $\rho_{\rm sat}/2$ to that of the crust EoS (Baym et al., 1971a,b). It is seen that the first hyperon to appear is the Λ , which is followed by the Ξ^- hyperon. The Σ^- hyperons do not appear because they are disfavored by their repulsive potential at nuclear saturation density (Bart et al., 1999; Dover and Gal, 1984; Gomes et al., 2015; Lopes and Menezes, 2014; Maslov et al., 2016; Miyatsu et al., 2015). Similar ordering of hyperon thresholds was found with other hypernuclear CDFs (Fortin et al., 2017; Li et al., 2018a,b; Weissenborn et al., 2012a,b); note also that this picture is in contrast to the case of free hyperonic gas, in which case Σ^- is, in fact, the first hyperon to nucleate (Ambartsumyan and Saakyan, 1960). The modification of the particle abundances in the cases when Δ 's are included is as follows (Li et al., 2018b). For strong enough Δ potential $V_{\Delta}^{(N)}$ the Δ -threshold density is considerably lower than that for the Λ hyperon. The larger $V_{\Delta}^{(N)}$ the

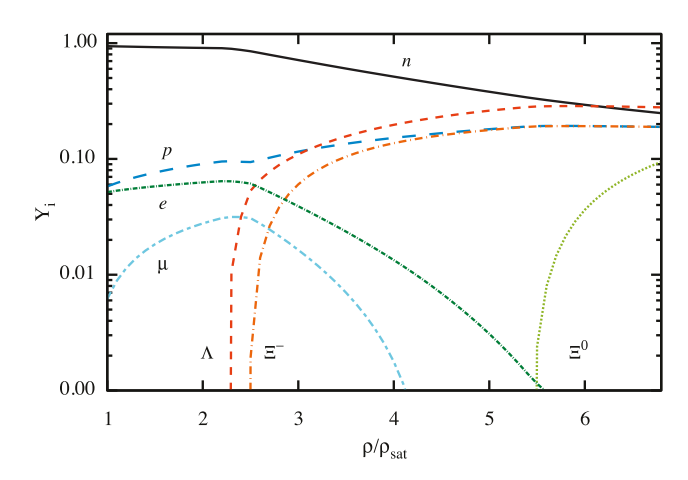


Fig. 5. Particle fractions $Y_i = n_i/n$, where n_i is the number density of species i and n is the total density, in zero-temperature hypernuclear matter according to the DDME2 model as a function of the ratio $\rho/\rho_{\rm sat}$.

lower is the onset densities of Δ 's. Because of its negative charge, the first Δ resonance to appear is the Δ^- , which competes with negatively charged leptons, effectively eliminates the Σ^- and shifts the threshold for the Ξ^- to higher densities. The Λ hyperon abundance is weakly affected by the Δ 's. For $V_{\Delta} \geq V_N$, the remaining $\Delta^{0,+,++}$ resonances also nucleate. By electric charge neutrality between the baryons and leptons, the appearance of negatively charged Δ^- and Ξ^- depletes the electron-muon population. Finally, for large $(V_{\Delta} \geq V_N)$ potentials Δ 's appear already in $1.4M_{\odot}$ compact stars.

4.2. Global static properties

The static properties of the compact stars in spherical symmetry (assuming no rotation and significant magnetic fields) are obtained from the integration of the Tolman-Oppenheimer-Volkoff equations (Oppenheimer and Volkoff, 1939; Tolman, 1939), which represent the solution of Einstein's equation for a spherically symmetrical distribution of mass. It is often useful to compare the theoretical predictions with the observations on plots that contain only observable quantities, i.e. combinations of mass, radius, the moment of inertia, spin frequency, etc. As an example, we show in

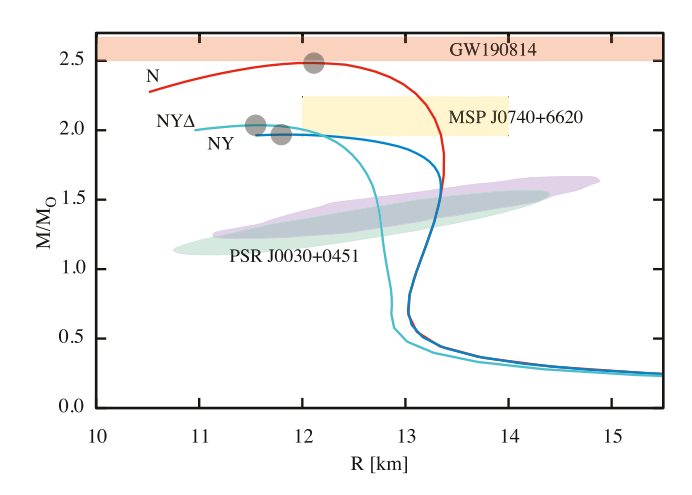


Fig. 6. MR relations for EoS of state with $N,\,NY,\,$ and $NY\Delta$ compositions. The shaded areas labeled PSR J0030+0451 corresponds to the 1σ constraints set by the NICER experiment (Miller et al., 2019; Riley et al., 2019). We also show the 2σ range mass for MSPJ0740+6620 (Cromartie et al., 2020) and the mass range extracted from the GW190814 event. The maximum mass for each stellar sequence is indicated by a solid dot

Fig. 6 the mass-radius (MR) relations for purely nucleonic, hyperonic, and hyperon- Δ admixed EoS presented in Fig. 4. The following observational constraints are included: (a) the 1σ constraints set by the NICER experiment on the mass and radius of PSR J0030+0451 (Miller et al., 2019; Riley et al., 2019); (b) the 2σ mass-limit on the largest millisecond pulsar MPS J0740+6620 mass measured (Cromartie et al., 2020) in combination with the recent NICER teams' report of its 1σ radius measurement in the range $12 \le R \le 14$ km (Miller et al., 2021; Riley et al., 2021); (c) the mass range inferred for the light companion of the binary observed in the GW190814 event to be discussed in detail in Sec. 5. The softening of the EoS when the heavy baryons are allowed is reflected in the significant reduction of the maximum mass of compact stars in both cases of only hyperons (NY)and hyperons and Δ -resonances $(NY\Delta)$. The additional softening of EoS at intermediate densities in the case when Δ -resonances are allowed results in a shift of the radius of the corresponding configuration to smaller values. Since in this case, the stiffness of the EoS is comparable to that of purely hyperonic matter at high densities (and even exceeds it asymptotically) the

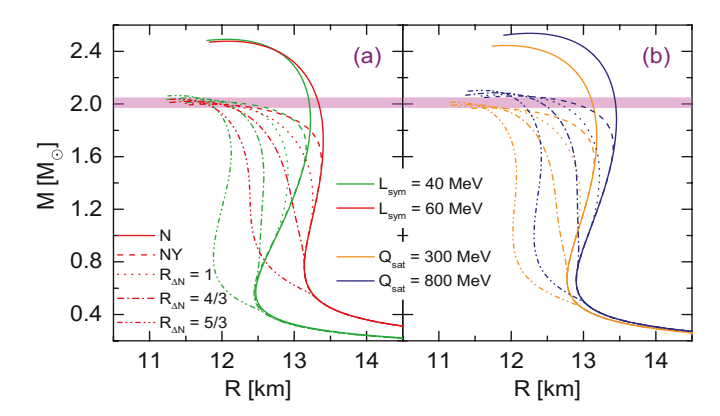


Fig. 7. Mass-radius relation for a set of EoS with varying $L_{\rm sym}$ (a) and $Q_{\rm sat}$ (b) and assuming purely nucleonic (N), hyperonic (NY), and hyperon- Δ admixed $(NY\Delta)$ compositions of stellar matter (Li and Sedrakian, 2019b). Three values of the Δ -potential have been used: $R_{\Delta N} = V_{\Delta}/V_N = 1$, 4/3 and 5/3, where V_N is the nucleon potential in isospin-symmetrical matter at saturation density.

values of the maximum masses $(M_{\rm max} \gtrsim 2.0 M_{\odot})$ are comparable in both cases of pure and Δ -admixed hypernuclear matter, see Fig. 6.

To illustrate the effect of variations of the nuclear characteristics on the mass and radius of compact stars Fig. 7 shows the MR plot for the three cases N, NY and NY Δ where the isoscalar $Q_{\rm sat}$, and the isovector $L_{\rm sym}$ characteristics are varied, while the remaining parameters in Eq. (36) are fixed at their values predicted by the DDME2 functional (see Table 3). Note that the variation of $Q_{\rm sat}$ is achieved by varying the three density-dependent parameters, i.e., these variations do not impact the meson-hyperon and meson- Δ couplings at nuclear saturation density. It is seen that smaller values of L_{sym} and Q_{sat} imply smaller radius for a given mass. At the same time, a smaller value of $Q_{\rm sat}$ predicts smaller maximal mass, as the high-density asymptotics of Eq. (36) is reduced. The effect of varying the Δ -meson couplings are shown by using various values of Δ potential $R_{\Delta N} =$ $V_{\Delta}(\rho_{\rm sat})/V_N(\rho_{\rm sat}) = 1;4/3;5/3$. It is seen that the larger is the value of $V_{\Delta}(\rho_{\rm sat})$ the smaller is the radius of the predicted configuration, as can be anticipated from the discussion of Fig. 6. Furthermore, the overall trends are rather similar when varying individually the characteristics for NY and $NY\Delta$ matter, as these are related to the properties of nuclear matter itself and not the heavy baryon admixture. The differences between the two compositions (i.e. NY vs $NY\Delta$) seen in Fig. 7 (e.g. in the radius of a canonical neutron star) arise from the factors that have been discussed in the context of Fig. 6. We close by noting that the parameter space used in Fig. 7 implies maximum masses of configurations larger than 2 M_{\odot} and radii within the range $12 \lesssim R \lesssim 14$ km independent of the composition.

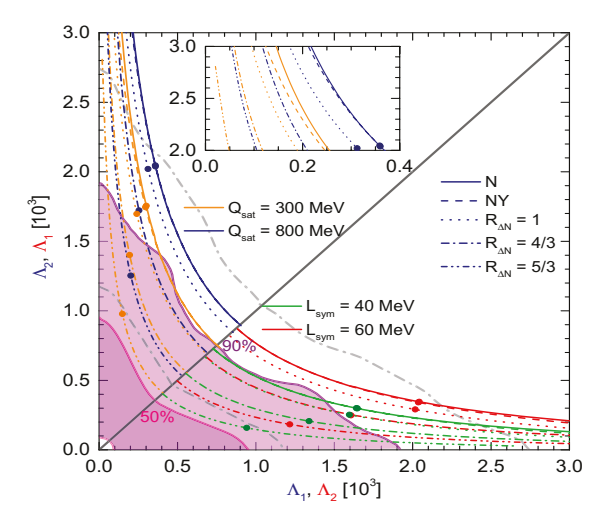


Fig. 8. Dimensionless tidal deformabilities extracted observationally from the GW170817 event (shaded areas) are compared with the predictions of EoS with various compositions and varying values of $L_{\rm sym}$, $Q_{\rm sat}$ and $R_{N\Delta}$ (Li and Sedrakian, 2019b). The light and heavy shadings correspond to the 50% and 90% credibility regions (Abbott et al., 2019). The results of the earlier analysis by LVC (Abbott et al., 2017) is shown by the gray dash-dotted curves. The dots correspond to the predictions for a BNS with mass ratio q=0.73.

4.3. Tidal deformabilities

Since the first observation of gravitational waves from a BNS merger - the GW170817 event - the tidal deformability of compact stars has become accessible observationally (Abbott *et al.*, 2017, 2019) and, thus, can be confronted with the theoretical predictions, as already indicated in Sec. 2. Figure 8 shows tidal deformabilities of two stars Λ_1 and Λ_2 as defined by Eq. (2) for N, NY, and $NY\Delta$ compositions, three values of the Δ -resonance potential in nuclear matter expressed through the ratio $R_{\Delta N} = V_{\Delta}/V_N$

and BNS member masses M_1 and M_2 . A variation in the characteristics is also allowed by varying $Q_{\rm sat}$ and $L_{\rm sym}$. The diagonal line corresponds to the case of an equal-mass binary assumption for GW170817 event, in which case $M_1 = M_2 = 1.362 M_{\odot}$. The light and heavily shaded areas represent the 90% and 50% confidence limits extracted from the analysis of GW170817 event (Abbott et al., 2019). It is seen that the data favors low values of $Q_{\rm sat} \simeq 300$ MeV and $L_{\rm sym} \simeq 40$ MeV for purely nucleonic compact stars, which are otherwise outside the allowed range. The inclusion of hyperons and Δ 's reduces the tidal deformability, as seen clearly from the inset in Fig. 8. The most significant reduction arises from the inclusion of the Δ 's with large attractive potential, i.e., large $R_{\Delta N}$ value. Thus, the appearance of Δ -resonances with reasonably attractive Δ -potential in the nuclear matter is needed to make the EoS models compatible with the data from GW170817. Purely hyperonic models are compatible with the 90% confidence limits for selected values of $Q_{\rm sat}$ and $L_{\rm sym}$. We note that the softening of EoS at intermediate densities caused by the onset of Δ 's is similar in its effect to a first-order phase transition to a quark matter in which case again more compact configurations arise, see, for example, Alford et al. (2013); Alford and Sedrakian (2017); Alvarez-Castillo et al. (2019); Alvarez-Castillo et al. (2019); Antić et al. (2021); Bonanno and Sedrakian (2012); Fukushima et al. (2020); Kojo (2020); Li et al. (2020a); Otto et al. (2020); Zdunik and Haensel (2013). In closing, we note that the information gained from MR and $\Lambda_1 - \Lambda_2$ relations are complementary to each other: different EoS models predicting different MR relations could feature $\Lambda_1 - \Lambda_2$ relations that are rather close to each other.

5. Rapidly Rotating Hyperonic Stars

A generic feature of Einstein's gravity is the existence of the maximum mass for compact stars assuming that the pressure originates from "ordinary" baryonic matter. The exact value of this maximum mass is currently unknown. Rotating compact stars accommodate larger masses than their static (non-rotating) counterparts by about 20% because the centrifugal force provides additional support against the gravitational pull towards the center of the star. There exist several public domain codes for computing stellar configurations of rapidly rotating compact stars (see the RNS code at Stergioulas (2003) and Gourgoulhon et al. (2021)). They are based on an iterative method of solution of Einstein's equations (Cook et al., 1994; Nozawa et al., 1998) in axial symmetry and use a tabulated EoS as an

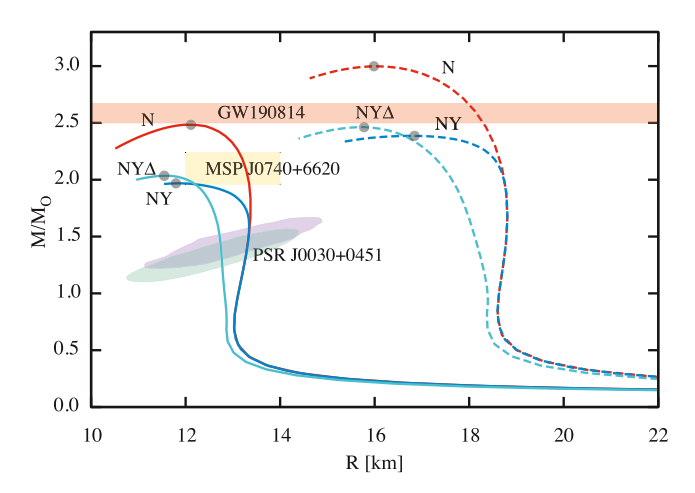


Fig. 9. The mass-radius relations for nonrotating (solid lines) and maximally rotating (dashed lines) nucleonic (N), hypernuclear (Y) and Δ -admixed-hypernuclear (Δ) stars. The colored areas show the constraints inferred from the most massive pulsar MSP J0740+6620 (Cromartie et al., 2020), the mass-radius limits inferred from the NICER experiment (Miller et al., 2019; Riley et al., 2019) and the mass limits from GW190814 (Abbott et al., 2020). The circles indicate the maximum masses of the sequences, to the left of which the stars are unstable.

input. The method of solution is iterative: it starts with a "guess" configuration (density profile), integrates the stellar structure equations, and uses this result as an input for a new iteration. This procedure is repeated until convergence to the desired accuracy is reached at each point of the spatial grid. Rotating compact stars with hyperonic cores have been considered in recent years as well (Haensel et al., 2016; Lenka et al., 2019). The interest in the exploration of rapidly rotating analogous of the models discussed in the previous sections arose after the measurement by the LVC (Abbott et al., 2020) of gravitational waves from a binary coalescence of a $24.3M_{\odot}$ black hole with a compact object in the mass the range of $2.50-2.67M_{\odot}$ (the GW190814 event). The light member of this binary has a mass that lies in the so-called "mass gap" $2.5 \lesssim M/M_{\odot} \lesssim 5$ where neither a neutron star nor a black hole has been observed and their existence is not obvious from the point of view of stellar evolution scenarios. A natural question that arises in this context is the possible compact star nature of the light companion. Below we discuss the conjecture that it could be a compact object which is rotating at a frequency that is close to the massshedding (Keplerian) limit (Li et al., 2020b; Sedrakian et al., 2020) based on an EoS which contains hyperons and Δ -resonances; see also Dexheimer et al. (2021a). Figure 9 shows the mass-radius relations of compact stars with three compositions N, NY and NY Δ based on the EoS with underlying DDME2 parametrization. The nucleonic models cover the mass range $2.48 \leq M/M_{\odot} \leq 3$ in the spin frequency range $0 \leq \Omega \leq \Omega_K$, where Ω_K is the Kepler frequency. Therefore, the nucleonic models account for the mass of a compact star in GW190814 even without rotation. In the case of NY and $NY\Delta$ compositions, the maximum masses (but not the radii) are quite similar in the static case and this feature extends to the case of rapidly rotating stars. As already noticed, the softening of the EoS in the case of NY and $NY\Delta$ compositions imply a lower maximum mass compared to the nucleonic case. The maximum masses for these compositions are close to $2.0M_{\odot}$, therefore the corresponding EoS are inconsistent with the compact star interpretation of the light companion in the GW190814 event. Their maximally rotating Keplerian analogs on the other hand have maximum masses $\leq 2.4 M_{\odot}$ suggesting that the maximal rotation is not sufficient to raise masses to the required value $2.5M_{\odot}$. Thus, there exists a significant tension between the hyperonization (with or without an admixture of Δ -resonances) and the interpretation of the light companion of GW190814 as a compact star. The results shown so far were obtained within a specific density functional and a valid question is whether the modifications of the CDF can alter this conclusion. A study of rapidly rotating stars in the case where the modifications of EoS of $NY\Delta$ matter were framed in the language of the characteristics appearing in Eq. (36), in particular the values of $Q_{\rm sat}$ and $L_{\rm sym}$ parameters, was carried out in Li et al. (2020b). The maximal value $R_{N\Delta} = 5/3$ was adopted although, as discussed above, the appearance of Δ -resonances increases the maximum mass of a configuration only slightly.

Figure 10 shows the dependence of maximum masses of the Keplerian models on parameters $Q_{\rm sat}$ and $L_{\rm sym}$ for $R_{N\Delta}=5/3$. It is seen that large masses, which are compatible with the compact star in GW190814, arise in the region of large $Q_{\rm sat}$ which imply larger energies at asymptotically large densities. Large masses are also favored for smaller values of parameter $L_{\rm sym}$ (which implies smaller radii of stars and, therefore, more compact objects). One may compare the required values of $Q_{\rm sat}$ with other existing functionals (to avoid, in a first approximation, a full-scale computation with any given functional). A comparison shows that the range of $Q_{\rm sat}$ values

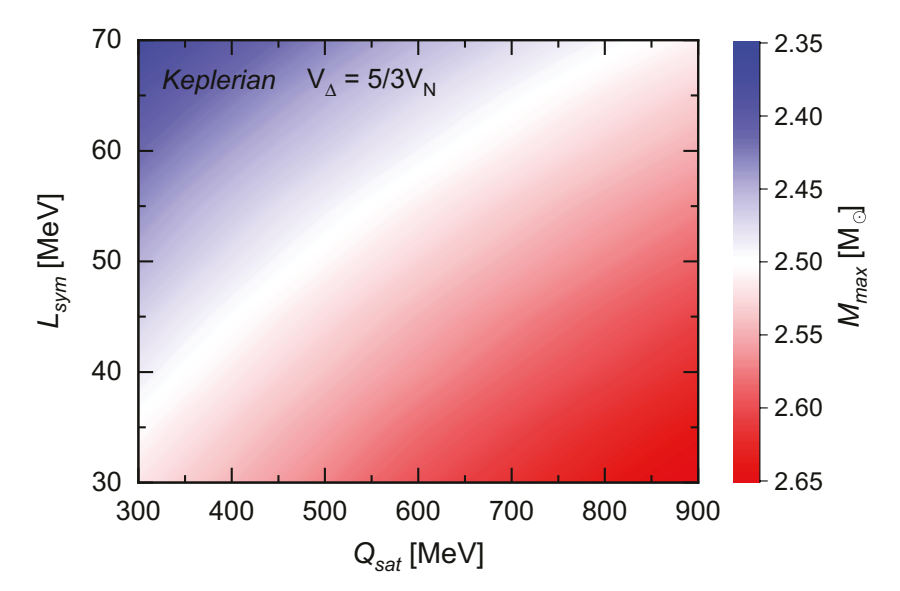


Fig. 10. The maximum masses of Keplerian sequences (color coded column on the right) as a function parameter space spanned by $Q_{\rm sat}$ and $L_{\rm sym}$. The Δ -resonance potential is fixed at assuming $R_{N\Delta}=5/3$. The large- $Q_{\rm sat}$ and small- $L_{\rm sym}$ range corresponds to compact stars with masses exceeding 2.5 M_{\odot} .

compatible with a compact star in GW190814 has no overlap with the values predicted by large samples of non-relativistic and relativistic density functionals (Dutra *et al.*, 2014, 2012), exceptions being the DDME2 (Lalazissis *et al.*, 2005) and some of the recently proposed functionals (Fattoyev *et al.*, 2020; Taninah *et al.*, 2020).

One may therefore conclude that the secondary object in GW190814 event must have been a low-mass black hole. The compact star interpretation is in strong tension with the idea of hyperonization of dense matter (with and without Δ -resonances). Several extreme assumptions are required to state the contrary, such as maximally rapid rotation, as well as $Q_{\rm sat}$ and $L_{\rm sym}$ values that are outside the range covered by most of the functionals.

6. Hyperonization vs Clustering at Low Densities

So far we concentrated on the hyperonization in the cold and dense matter as it occurs in the mature compact stars, where the appearance of hyperons was made energetically favorable by the fact that in the compressed matter the neutron Fermi energy can exceed the in-medium rest masses of various hyperons. However, thermodynamic conditions may be favorable for the hyperonization in a different setting, such as in dilute and warm matter that may be (transiently) formed in supernova explosions and BNS mergers (Nakazato et al., 2012; Peres et al., 2013). Because under these conditions nuclear matter is composed of nucleons and clusters (characterized by a mass number and a charge) at certain isospin asymmetry one needs to resort to the ideas of nuclear statistical equilibrium (Avancini et al., 2017; Botvina and Mishustin, 2010; Furusawa and Mishustin, 2017; Grams et al., 2018; Gulminelli and Raduta, 2012, 2015; Hempel et al., 2012, 2015; Pais et al., 2020; Raduta and Gulminelli, 2010, 2019; Röpke, 2020; Typel et al., 2010; Zhang and Chen, 2019). Additional facets are the pionization (at sufficiently high temperatures) (Colucci et al., 2014; Fore and Reddy, 2020; Ishizuka et al., 2008; Peres et al., 2013) and formation of condensates of deuterons (Lombardo et al., 2001; Sedrakian and Clark, 2006; Sedrakian and Clark, 2019) and alpha-particles (Furusawa and Mishustin, 2020; Satarov et al., 2019, 2021; Wu et al., 2017; Zhang and Chen, 2017, 2019) at low temperatures.

An interesting question to be explored is the interplay between the clustering and heavy-baryon degrees of freedom in dilute, finite-temperature nuclear matter (Fortin et al., 2018; Menezes and Providência, 2017; Sedrakian, 2020). The rich nucleon- Δ -pion dynamics, extensively explored in the heavy-ion context, suggests that one needs to include the quartet of Δ -resonances and the isotriplet of pions $\pi^{\pm,0}$ along with the nucleons and clusters (Sedrakian, 2020). In a first approximation, the full nuclear statistical ensemble can be approximated by the light clusters with the mass number A < 4 and a heavy nucleus, for example, ⁵⁶Fe. Since the hyperonic interactions are less important at low densities the lightest Λ -hyperon is expected to contribute dominantly to the strangeness content of matter. As an illustrative example we show in Fig. 11 the composition of dilute nuclear matter in the temperature range $10 \le T \le 30$ MeV and density $10^{-2} \rho_{\rm sat}$ for charge fractions $Y_Q = 0.4$ (characteristic for supernova matter) and $Y_{\mathcal{O}} = 0.1$ (characteristic for BNS mergers) (Sedrakian, 2020). We show the mass fraction $X_j = A_j n_j / n$, where A_j is the mass number of a constituent, n_i is their number density, and n is the total density. The mass fraction of ⁵⁶Fe is not visible on the figure's scale. The main observation is that there is a transition from light baryons and clusters to heavy-baryon featuring matter at about temperature $T_{\rm tr} \sim 30$ MeV. Once heavy baryons and pions

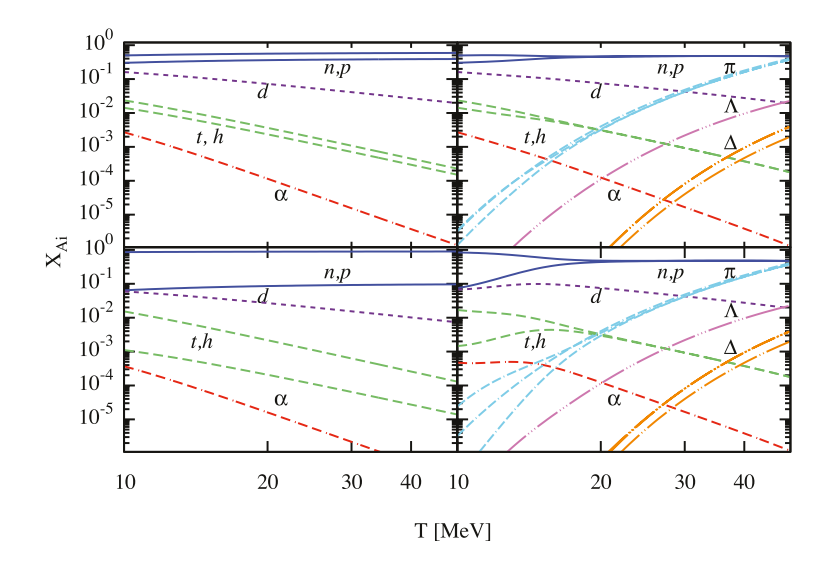


Fig. 11. Mass fractions of the constituents as a function of temperature at fixed density $10^{-2}\rho_{\rm sat}$ for charge fractions $Y_Q=0.4$ (top panels) and 0.1 (bottom panels). In the two left panels include only nucleons and light clusters, whereas the two right panels the full composition. The composition includes neutrons n, protons p, deuterons d, triton t helium h, α -particles, Δ resonances, Λ -hyperon and pions π .

are included the isospin asymmetry in the neutron and proton components is reduced. This affects the abundances of the helion and triton which are then closer together. We believe that these are generic, model-independent features. The transition temperature itself is dependent on the treatment of the interactions and assumed composition; for alternatives see Fortin et al. (2018); Menezes and Providência (2017). Other generic aspects worth mentioning are: (a) in the presence of a heavy nucleus the abundances of light clusters are strongly suppressed at low temperatures; (b) the phase-space occupation suppresses completely the light clusters for densities $\geq 0.1 \rho_{\rm sat}$ due to the Pauli blocking (Röpke, 2020); (c) at low enough temperatures deuterons can cross-over from Bose-Einstein to Bardeen-Cooper-Schrieffer pair condensate (Lombardo et al., 2001; Sedrakian and Clark, 2006; Sedrakian and Clark, 2019).

7. Hypernuclear Stars: pairing patterns and cooling

The long-term cooling of compact stars is a sensitive probe of the interior composition of such stars (Page, 2009; Page et al., 2006; Potekhin, 2010; Schaab et al., 1996; Sedrakian, 2007; Shapiro and Teukolsky, 1983). It is characterized by neutrino emission from the bulk of the stellar interior during the time-span $t \leq 10^5$ yr after the star's birth, which is followed by late-time photon cooling from its surface, assuming that there is no internal heating mechanism operating at any stage of evolution. With the advent of CDFs which were tuned to reproduce the available astrophysical and laboratory data, it became feasible to perform simulations of cooling of compact stars with hyperonization in a more constrained manner than was possible initially (Fortin et al., 2021; Grigorian et al., 2018; Negreiros et al., 2018; Raduta et al., 2019, 2017).

Hyperonic matter cools via the direct Urca processes (Prakash *et al.*, 1992). There exist density thresholds for these processes to operate, which are dictated by the kinematics involved in the reaction, but these densities are very low for hyperons, i.e., they start operating at a density that is slightly above the onset density for a hyperon participating in a reaction. Baryon pairing is known to suppress the rates of the Urca (and other baryonic) processes, therefore another unknown in the cooling simulations is the magnitude of the gaps in the spectra of various hyperons (Raduta *et al.*, 2019, 2017).

Nevertheless, with the input provided by any given CDF which can be supplemented by the solutions of the BCS equations for the hyperons, the simulations of the cooling of compact stars provided some generic insights (Raduta et al., 2019, 2017). There appears to be a mass hierarchy with respect to the cooling behavior. The lightest stars that contain hyperons with $M/M_{\odot} \gtrsim 1.5$ cool via the Urca process $\Lambda \to p + l + \bar{\nu}_l$, where lstands for lepton, $\bar{\nu}_l$ for the associated antineutrino. The appearance of $\Xi^$ in slightly more massive stars opens a competing channel via $\Xi^- \to \Lambda + l + \bar{\nu}_l$, the degree of its efficacy depending on the pairing gaps of Ξ^- . For very massive stars with $M/M_{\odot} \sim 2$ the S-wave gaps of protons and Λ 's will vanish at high densities (because the interactions will become repulsive at large energies) and therefore the Urca process involving Λ, p baryons will be the dominant one. Simulations show that the massive is the star the faster it cools. If Σ^- appears in the matter, the corresponding Urca process via Λ hyperon may be the dominant cooling agent, since Σ^- interaction is likely repulsive with no BCS gap in their spectrum. Given the mass hierarchy, the observations of the surface temperatures of neutron stars can be explained by the variation of their masses within their population (the light objects are hot, the heavier ones – cold). Note that the massive models may not develop normal cores of hyperons due to the possible pairing in the P-wave channel in the high-density matter in which case fast cooling will not take place (Raduta et al., 2019). The pairing in the hyperonic sector remains the main unknown for cooling simulations of hypernuclear stars. Given this uncertainty, some studies neglect the hyperonic pairing altogether (Grigorian et al., 2018; Negreiros et al., 2018).

There are uncertainties in the studies of cooling of neutron stars, that are unrelated to the hyperonic component, which we list here for completeness. These include the composition of the atmosphere (Potekhin et al., 2020) which substantially affects the surface temperature of the star and the pairing gaps of neutrons and protons in the domains where interactions are attractive (Sedrakian and Clark, 2019). Large magnetic fields are a factor, as they dissipate sufficient energy to heat up the star (Viganò et al., 2021).

8. Universal Relations

In recent years universal relations among the global properties of compact stars were established under various conditions, including stationary (non-rotating), rigidly rotating, magnetized, and finite-temperature stars, for a review, see Yagi and Yunes (2017). The universality of relations between global parameters refers to their independence of the EoS that has been input to compute them. These have proven to be rather useful for the interpretation of observational data because they reduce the uncertainties which are related to the EoS.

In the case of hypernuclear stars (with and without Δ -resonances) it has been established that the universality is maintained among the moment of inertia, quadruple moment and the Love number of the star (the so-called I-Love-Q relations) and the dependence of the moment of inertia, quadrupole moment, tidal deformability on the compactness in cold (Lenka et al., 2017) and warm neutron stars (Raduta et al., 2020). Their extension to finite temperature poses some challenges: it turns out that universalities are maintained if one considers stars at the same entropy per baryon S/A and lepton fraction (Raduta et al., 2020), otherwise the universality is lost (Marques et al., 2017; Maselli et al., 2013). Clearly, constant entropy approximation will break down under realistic conditions to some degree.

While we can be certain that there are no physical obstacles to maintaining the universality in the finite-temperature domain, a formulation that accounts for entropy gradients needs to be tested. The universalities so far established extend further to the rapidly rotating stars at finite temperature without loss of accuracy (Khadkikar *et al.*, 2021).

9. Concluding Remarks

The hyperonization of dense matter and the astrophysics of compact stars featuring hyperons and Δ -resonances is a vivid field of research with a strong relation to the observational multimessenger astronomy of compact stars. The recent advances on the observational front, which include the observation of gravitational waves from BNS mergers, notably GW170817, simultaneous measurement of masses and radii of neutron stars and the discovery of very massive pulsars motivate further improvements of the existing models and exploration of their new implications in novel astrophysical scenarios. The ongoing and future hypernuclear programs at CERN, BNL, JLab, GSI-FAIR, and J-PARC, and elsewhere will eventually provide us with insights on hypernuclei as they occur in terrestrial laboratories. These can be used to narrow down the parameters of the CDFs and constrain other theoretical models. The results achieved so far indicate that the combination of theoretical work with the observational advances has the potential of revealing the detailed features of the high-density matter found in compact stars in the observable future.

Acknowledgements

We are grateful to M. Alford, A. Harutyunyan, M. Oertel, A. Raduta, M. Sinha, V. Thapa for collaboration and insights on the topics related to this chapter. A. S. acknowledges the support by the Deutsche Forschungsgemeinschaft (Grant No. SE 1836/5-1) and the European COST Action CA16214 PHAROS "The multi-messenger physics and astrophysics of neutron stars". F. W. is supported through the U.S. National Science Foundation under Grants PHY-1714068 and PHY-2012152.

References

Abbott, B. P., Abbott, R., Abbott, T. D., Acernese, F., Ackley, K., et al. (2017).
GW170817: Observation of gravitational waves from a binary neutron star

- inspiral, Phys. Rev. Lett. 119, pp. 161101.
- Abbott, B. P., Abbott, R., Abbott, T. D., Acernese, F., Ackley, K., et al. (2019). Properties of the Binary Neutron Star Merger GW170817, Phys. Rev. X 9, pp. 011001.
- Abbott, B. P. e. a. (2020). GW190425: Observation of a compact binary coalescence with total mass $\sim 3.4~M_{\odot}$, Ap. J. Lett 892, p. L3.
- Abbott, R. et al. (2020). GW190814: Gravitational waves from the coalescence of a 23 solar mass black hole with a 2.6 solar mass compact object, Ap. J. 896, pp. L44.
- Alberico, W. M., Gervino, G., and Lavagno, A. (1994). Phenomenological Approach to Baryon Resonance Damping in Nuclei, Phys. Lett. B 321, pp. 177–182.
- Alford, M. G., Han, S., and Prakash, M. (2013). Generic Conditions for Stable Hybrid Stars, Phys. Rev. D 88, pp. 083013.
- Alford, M. G. and Sedrakian, A. (2017). Compact Stars With Sequential Qcd Phase Transitions, Phys. Rev. Lett. 119, p. 161104.
- Altaha Motahar, Z., Blázquez-Salcedo, J. L., Kleihaus, B., and Kunz, J. (2017). Scalarization of Neutron Stars With Realistic Equations of State, Phys. Rev. D 96, p. 064046.
- Alvarez-Castillo, D. E., Antoniadis, J., Ayriyan, A., Blaschke, D., Danchev, V., Grigorian, H., Largani, N. K., and Weber, F. (2019). Accretion-induced Collapse to Third Family Compact Stars as Trigger for Eccentric Orbits of Millisecond Pulsars in Binaries, Astronomische Nachrichten 340, pp. 878–884.
- Alvarez-Castillo, D. E., Blaschke, D. B., Grunfeld, A. G., and Pagura, V. P. (2019). Third Family of Compact Stars within a Nonlocal Chiral Quark Model Equation of State, Phys. Rev. D 99, p. 063010.
- Ambartsumyan, V. A. and Saakyan, G. S. (1960). The Degenerate Superdense Gas of Elementary Particles, Soviet Astronomy 4, p. 187.
- Ambartsumyan, V. A. and Saakyan, G. S. (1961). On Equilibrium Configurations of Superdense Degenerate Gas Masses, Astronomicheskii Zhurnal 38, p. 785.
- Antić, S., Shahrbaf, M., Blaschke, D., and Grunfeld, A. G. (2021). Parameter Mapping Between the Microscopic Nonlocal Nambu Jona-Lasinio and Constant Sound Speed Models, http://arxiv.org/abs/2105.00029 (arXiv:2105.00029 [nucl-th]).
- Antoniadis, J., Freire, P. C. C., Wex, N., Tauris, T. M., Lynch, R. S., van Kerkwijk, M. H., Kramer, M., Bassa, C., Dhillon, V. S., Driebe, T., Hessels, J. W. T., Kaspi, V. M., Kondratiev, V. I., Langer, N., Marsh, T. R., McLaughlin, M. A., Pennucci, T. T., Ransom, S. M., Stairs, I. H., van Leeuwen, J., Verbiest, J. P. W., and Whelan, D. G. (2013). A Massive Pulsar in a Compact Relativistic Binary, Science 340, p. 448.
- Astashenok, A. V., Capozziello, S., and Odintsov, S. D. (2014). Maximal Neutron Star Mass and the Resolution of the Hyperon Puzzle in Modified Gravity, Phys. Rev. D 89, p. 103509.
- Astashenok, A. V., Capozziello, S., and Odintsov, S. D. (2015a). Extreme neutron

- stars from Extended Theories of Gravity, JCAP 01, p. 001.
- Astashenok, A. V., Capozziello, S., and Odintsov, S. D. (2015b). Magnetic Neutron Stars in f(R) Gravity, Astrophys. Space Sci. 355, pp. 333–341.
- Avancini, S. S., Ferreira, M., Pais, H., Providência, C., and Röpke, G. (2017).
 Light Clusters and Pasta Phases in Warm and Dense Nuclear Matter, Phys. Rev. C 95, p. 045804.
- Baiotti, L. (2019). Gravitational Waves from Neutron Star Mergers and their Relation to the Nuclear Equation of State, Prog. Part. Nucl. Phys. 109, p. 103714.
- Baldo, M., Burgio, G. F., and Schulze, H.-J. (2000). Hyperon Stars in the Brueckner-bethe-goldstone Theory, Phys. Rev. C 61, p. 055801.
- Banik, S., Hempel, M., and Bandyopadhyay, D. (2014). New Hyperon Equations of State for Supernovae and Neutron Stars in Density-dependent Hadron Field Theory, Ap. J. Suppl. 214, p. 22.
- Bardeen, J. M., Thorne, K. S., and Meltzer, D. W. (1966). A Catalogue of Methods for Studying the Normal Modes of Radial Pulsation of General-Relativistic Stellar Models, Ap. J. 145, p. 505.
- Bart, S., Chrien, R. E., Franklin, W. A., Fukuda, T., Hayano, R. S., Hicks, K., Hungerford, E. V., Michael, R., Miyachi, T., Nagae, T., Nakano, J., Naing, W., Omata, K., Sawafta, R., Shimizu, Y., Tang, L., and Wissink, S. W. (1999). Σ Hyperons in the Nucleus, Phys. Rev. Lett. 83, pp. 5238–5241.
- Baym, G., Bethe, H. A., and Pethick, C. J. (1971a). Neutron Star Matter, Nucl. Phys. A 175, 2, pp. 225–271.
- Baym, G., Pethick, C., and Sutherland, P. (1971b). The Ground State of Matter at High Densities: Equation of state and stellar models, Ap. J. 170, p. 299.
- Bednarek, I., Haensel, P., Zdunik, J. L., Bejger, M., and Manka, R. (2012). Hyperons in Neutron-star Cores and Two-solar-mass Pulsar, Astronomy & Astrophysics 543, p. A157.
- Blaschke, D. and Chamel, N. (2018). Phases of Dense Matter in Compact Stars, Astrophys. Space Sci. Libr. 457, pp. 337–400.
- Blázquez-Salcedo, J. L., González-Romero, L. M., Kunz, J., Mojica, S., and Navarro-Lérida, F. (2016). Axial Quasinormal Modes of Einstein-Gauss-Bonnet-dilaton Neutron Stars, Phys. Rev. D 93, p. 024052.
- Bombaci, I. (2017). The Hyperon Puzzle in Neutron Stars, JPS Conf. Proc. 17, p. 101002.
- Bonanno, L. and Sedrakian, A. (2012). Composition and Stability of Hybrid Stars with Hyperons and Quark Color-superconductivity, Astronomy & Astrophysics 539, p. A16.
- Botvina, A. S. and Mishustin, I. N. (2010). Statistical Approach for Supernova Matter, Nucl. Phys. A 843, pp. 98–132.
- Cai, B.-J. and Chen, L.-W. (2017). Constraints on the Skewness Coefficient of Symmetric Nuclear Matter Within the Nonlinear Relativistic Mean Field Model, Nucl. Sci. Tech. 28, p. 185.
- Cai, B.-J., Fattoyev, F. J., Li, B.-A., and Newton, W. G. (2015). Critical Density and Impact of Δ(1232) Resonance Formation in Neutron Stars, Phys. Rev. C 92, p. 015802.

- Cai, B.-J. and Li, B.-A. (2021). Intrinsic Correlations Among Characteristics of Neutron-rich Matter Imposed by the Unbound Nature of Pure Neutron Matter, Phys. Rev. C 103, p. 034607.
- Chatterjee, D. and Vidaña, I. (2016). Do Hyperons Exist in the Interior of Neutron Stars? Eur. Phys. J. A 52, p. 29.
- Choudhury, S. K. and Rakshit, R. (1993). Δ-excited Nuclear Matter in the Derivative Scalar Coupling Model, Phys. Rev. C 48, pp. 598–601.
- Collins, J. C. and Perry, M. J. (1975). Superdense Matter: Neutrons or asymptotically free quarks? Phys. Rev. Lett. 34, pp. 1353–1356.
- Colucci, G., Fraga, E. S., and Sedrakian, A. (2014). Chiral Pions in a Magnetic Background, Phys. Lett. B 728, pp. 19–24.
- Colucci, G. and Sedrakian, A. (2013). Equation of State of Hypernuclear Matter: Impact of hyperon-scalar-meson couplings, Phys. Rev. C 87, p. 055806.
- Cook, G. B., Shapiro, S. L., and Teukolsky, S. A. (1994). Rapidly Rotating Neutron Stars in General Relativity: Realistic Equations of State, Ap. J. 424, p. 823.
- Cozma, M. D. (2016). The Impact of Energy Conservation in Transport Models on the π⁻/π⁺ Multiplicity Ratio in Heavy-ion Collisions and the Symmetry Energy, Phys. Lett. B 753, pp. 166–172.
- Cozma, M. D. and Tsang, M. B. (2021). In-medium \(\Delta(1232) \) Potential, Pion Production in Heavy-ion Collisions and the Symmetry Energy, http://arxiv.org/abs/2101.08679 (arXiv:2101.08679 [nucl-th]).
- Cromartie, H. T., Fonseca, E., Ransom, S. M., Demorest, P. B., Arzoumanian, Z.,
 Blumer, H., Brook, P. R., DeCesar, M. E., Dolch, T., Ellis, J. A., Ferdman,
 R. D., Ferrara, E. C., Garver-Daniels, N., Gentile, P. A., Jones, M. L., Lam,
 M. T., Lorimer, D. R., Lynch, R. S., McLaughlin, M. A., Ng, C., Nice,
 D. J., Pennucci, T. T., Spiewak, R., Stairs, I. H., Stovall, K., Swiggum,
 J. K., and Zhu, W. W. (2020). Relativistic Shapiro Delay Measurements of
 an Extremely Massive Millisecond Pulsar, Nature Astronomy 4, pp. 72–76.
- de Swart, J. J. (1963). The Octet Model and its Clebsch-Gordan Coefficients, Rev. Mod. Phys. 35, pp. 916–939.
- Demorest, P. B., Pennucci, T., Ransom, S. M., Roberts, M. S. E., and Hessels, J. W. T. (2010). A Two-solar-mass Neutron Star Measured Using Shapiro delay, Nature 467, pp. 1081–1083.
- Dexheimer, V., Gomes, R. O., Klähn, T., Han, S., and Salinas, M. (2021a). GW190814 as a Massive Rapidly Rotating Neutron Star with Exotic Degrees of Freedom, Phys. Rev. C 103, p. 025808.
- Dexheimer, V., Marquez, K. D., and Menezes, D. P. (2021b). *Delta Baryons in Neutron-Star Matter under Strong Magnetic Fields*, http://arxiv.org/abs/2103.09855 (arXiv:2103.09855 [nucl-th]).
- Dover, C. and Gal, A. (1984). Hyperon-nucleus Potentials, Prog. Part. Nucl. Phys. 12, pp. 171–239.
- Drago, A., Lavagno, A., Pagliara, G., and Pigato, D. (2014). Early Appearance of Δ Isobars in Neutron Stars, Phys. Rev. C **90**, p. 065809.
- Drago, A., Lavagno, A., Pagliara, G., and Pigato, D. (2016). The scenario of two families of compact stars: 1. Equations of State, Mass-radius Relations and

- Binary Systems, Eur. Phys. J. A 52, p. 40.
- Dutra, M., Lourenço, O., Avancini, S. S., Carlson, B. V., Delfino, A., Menezes, D. P., Providência, C., Typel, S., and Stone, J. R. (2014). Relativistic Meanfield Hadronic Models Under Nuclear Matter Constraints, Phys. Rev. C 90, p. 055203.
- Dutra, M., Lourenço, O., Sá Martins, J. S., Delfino, A., Stone, J. R., and Stevenson, P. D. (2012). Skyrme Interaction and Nuclear Matter Constraints, Phys. Rev. C 85, p. 035201.
- Fattoyev, F. J., Horowitz, C. J., Piekarewicz, J., and Reed, B. (2020). GW190814: Impact of a 2.6 Solar Mass Neutron Star on the Nucleonic Equations of State, Phys. Rev. C 102, p. 065805.
- Flanagan, E. E. and Hinderer, T. (2008). Constraining Neutron-star Tidal Love Numbers with Gravitational-wave Detectors, Phys. Rev. D 77, p. 021502.
- Fonseca, E., Cromartie, H. T., Pennucci, T. T., Ray, P. S., Kirichenko, A. Y., Ransom, S. M., Demorest, P. B., Stairs, I. H., Arzoumanian, Z., Guillemot, L., Parthasarathy, A., Kerr, M., Cognard, I., Baker, P. T., Blumer, H., Brook, P. R., DeCesar, M., Dolch, T., Dong, F. A., Ferrara, E. C., Fiore, W., Garver-Daniels, N., Good, D. C., Jennings, R., Jones, M. L., Kaspi, V. M., Lam, M. T., Lorimer, D. R., Luo, J., McEwen, A., McKee, J. W., McLaughlin, M. A., McMann, N., Meyers, B. W., Naidu, A., Ng, C., Nice, D. J., Pol, N., Radovan, H. A., Shapiro-Albert, B., Tan, C. M., Tendulkar, S. P., Swiggum, J. K., Wahl, H. M., and Zhu, W. (2021). Refined Mass and Geometric Measurements of the High-Mass PSR J0740+6620, http://arxiv.org/abs/2104.00880 (arXiv:2104.00880 [astro-ph.HE]).
- Fonseca, E., Pennucci, T. T., Ellis, J. A., Stairs, I. H., Nice, D. J., Ransom, S. M., Demorest, P. B., Arzoumanian, Z., Crowter, K., Dolch, T., Ferdman, R. D., Gonzalez, M. E., Jones, G., Jones, M. L., Lam, M. T., Levin, L., McLaughlin, M. A., Stovall, K., Swiggum, J. K., and Zhu, W. (2016). The NANOGrav Nine-year Data Set: Mass and Geometric Measurements of Binary Millisecond Pulsars, Ap. J. 832, p. 167.
- Fore, B. and Reddy, S. (2020). Pions in Hot Dense Matter and their Astrophysical Implications, Phys. Rev. C 101, p. 035809.
- Fortin, M., Avancini, S. S., Providência, C., and Vidaña, I. (2017). Hypernuclei and Massive Neutron Stars, Phys. Rev. C 95, p. 065803.
- Fortin, M., Oertel, M., and Providência, C. (2018). Hyperons in Hot Dense Matter: What do the constraints tell us for equation of state? PASA 35, p. 44.
- Fortin, M., Raduta, A. R., Avancini, S., and Providência, C. (2020). Relativistic Hypernuclear Compact Stars with Calibrated Equations of State, Phys. Rev. D 101, p. 034017.
- Fortin, M., Raduta, A. R., Avancini, S., and Providência, C. (2021). Thermal Evolution of Relativistic Hyperonic Compact Stars with Calibrated Equations of State, Phys. Rev. D 103, p. 083004.
- Friedman, E. and Gal, A. (2021). Constraints on Ξ^- Nuclear Interactions from Capture Events in Emulsion, http://arxiv.org/abs/2104.00421 (arXiv:2104.00421 [nucl-th]).
- Fukushima, K., Kojo, T., and Weise, W. (2020). Hard-core Deconfinement and

- Soft-surface Delocalization from Nuclear to Quark Matter, Phys. Rev. D 102, p. 096017.
- Furusawa, S. and Mishustin, I. (2017). Self-consistent Calculation of the Nuclear Composition in Hot and Dense Stellar Matter, Phys. Rev. C 95, p. 035802.
- Furusawa, S. and Mishustin, I. (2020). Degeneracy Effects and Bose Condensation in Warm Nuclear Matter with Light and Heavy Clusters, Nuclear Physics A 1002, p. 121991.
- Gandolfi, S. and Lonardoni, D. (2017). The EOS of Neutron Matter and the Effect of Λ Hyperons to Neutron Star Structure, JPS Conf. Proc. 17, p. 101001.
- Glendenning, N. (2012). Compact Stars: Nucl. Phys., Particle Physics and General Relativity, Astronomy and Astrophysics Library (Springer New York), ISBN 9781468404913.
- Glendenning, N. K. (1985). Neutron Stars are Giant Hypernuclei? Ap. J. 293, 1, pp. 470–493.
- Glendenning, N. K. and Moszkowski, S. A. (1991). Reconciliation of Neutron Star Masses and Binding of the Lambda in Hypernuclei, Phys. Rev. Lett. 67, pp. 2414–2417.
- Glendenning, N. K., Weber, F., and Moszkowski, S. A. (1992). Neutron and Hybrid Stars in the Derivative Coupling Model, Phys. Rev. C 45, pp. 844– 855.
- Gomes, R. O., Char, P., and Schramm, S. (2019). Constraining Strangeness in Dense Matter with GW170817, Ap. J. 877, p. 139.
- Gomes, R. O., Dexheimer, V., Schramm, S., and Vasconcellos, C. A. Z. (2015).
 Many-body Forces in the Equation of State of Hyperonic Matter, Ap. J.
 808. p. 8.
- Grams, G., Giraud, S., Fantina, A. F., and Gulminelli, F. (2018). Distribution of Nuclei in Equilibrium Stellar Matter from the Free-energy Density in a Wigner-Seitz Cell, Phys. Rev. C 97, p. 035807.
- Grigorian, H., Voskresensky, D. N., and Maslov, K. A. (2018). Cooling of Neutron Stars in "Nuclear Medium Cooling Scenario" with Stiff Equation of State Including Hyperons, Nucl. Phys. A 980, pp. 105–130.
- Gulminelli, F. and Raduta, A. R. (2012). Ensemble Inequivalence in Supernova Matter within a Simple Model, Phys. Rev. C 85, p. 025803.
- Gulminelli, F. and Raduta, A. R. (2015). Unified Treatment of Subsaturation Stellar Matter at Zero and Finite Temperature, Phys. Rev. C 92, p. 055803.
- Gusakov, M. E., Haensel, P., and Kantor, E. M. (2014). Physics Input for Modelling Superfluid Neutron Stars with Hyperon Cores, Mon. Not. Roy. Astron. Soc. 439, pp. 318–333.
- Güven, H., Bozkurt, K., Khan, E., and Margueron, J. (2018). ΛΛ Pairing in Multi-strange Hypernuclei, Phys. Rev. C 98, 1, p. 014318.
- Haensel, P., Bejger, M., Fortin, M., and Zdunik, L. (2016). Rotating Neutron Stars with Exotic Cores: Masses, radii, stability, Eur. Phys. J. A 52, p. 59.
- Haidenbauer, J., Meißner, U. G., Kaiser, N., and Weise, W. (2017). Lambdanuclear Interactions and Hyperon Puzzle in Neutron Stars, Eur. Phys. J. A 53, p. 121.
- Hempel, M., Fischer, T., Schaffner-Bielich, J., and Liebendörfer, M. (2012). New

- Equations of State in Simulations of Core-collapse Supernovae, Ap. J. 748, p. 70.
- Hempel, M., Hagel, K., Natowitz, J., Röpke, G., and Typel, S. (2015). Constraining Supernova Equations of State with Equilibrium Constants from Heavy-ion Collisions, Phys. Rev. C 91, p. 045805.
- Horikawa, Y., Thies, M., and Lenz, F. (1980). The Δ-nucleus Spin-orbit Interaction in π-nucleus Scattering, Nuclear Physics A 345, pp. 386–408.
- Huber, H., Weber, F., and Weigel, M. K. (1994). Neutron Star Properties and the Relativistic Equation of State of Asymmetric Nuclear Matter, Phys. Rev. C 50, pp. R1287–R1291.
- Huber, H., Weber, F., Weigel, M. K., and Schaab, C. (1998). Neutron Star Properties with Relativistic Equations of State, Int. J. Mod. Phys. E 7, 03, pp. 301–339
- Inoue, T. and HAL QCD Collaboration (2019). Strange Nuclear Physics from QCD on Lattice, in The 13th International Conference on HyperNuclear and Strange Particle Physics: HYP2018, American Institute of Physics Conference Series, Vol. 2130, p. 020002.
- Ishizuka, C., Ohnishi, A., Tsubakihara, K., Sumiyoshi, K., and Yamada, S. (2008). Tables of Hyperonic Matter Equation of State for Core-collapse Supernovae, J. Nucl. Phys. G 35, p. 085201.
- Itoh, N. (1970). Hydrostatic Equilibrium of Hypothetical Quark Stars, Progress of Theoretical Physics 44, pp. 291–292.
- Jiang, W.-Z., Li, B.-A., and Chen, L.-W. (2012). Large-mass Neutron Stars with Hyperonization, Ap. J. 756, p. 56.
- Khadkikar, S., Raduta, A. R., Oertel, M., and Sedrakian, A. (2021). Maximum Mass of Compact Stars from Gravitational Wave Events with Finite-temperature Equations of State, Phys. Rev. C 103, p. 055811.
- Khan, E., Margueron, J., Gulminelli, F., and Raduta, A. R. (2015). Microscopic Evaluation of the Hypernuclear Chart with Λ Hyperons, Phys. Rev. C 92, 4, p. 044313, doi:10.1103/PhysRevC.92.044313, http://arxiv.org/abs/ 1505.07678 (arXiv:1505.07678 [nucl-th]).
- Koch, V. (1997). Aspects of Chiral Symmetry, Int. J. Mod. Phys. E 6, pp. 203–250.
- Kojo, T. (2020). QCD Equations of State and Speed of Sound in Neutron Stars, http://arxiv.org/abs/2011.10940 (arXiv:2011.10940 [nucl-th]).
- Kolomeitsev, E. E., Maslov, K. A., and Voskresensky, D. N. (2017). Delta Isobars in Relativistic Mean-field Models with σ-scaled Hadron Masses and Couplings, Nucl. Phys. A 961, pp. 106–141.
- Lalazissis, G. A., Nikšić, T., Vretenar, D., and Ring, P. (2005). New Relativistic Mean-field Interaction with Density-dependent Meson-nucleon Couplings, Phys. Rev. C 71, p. 024312.
- Lattimer, J. M. (2019). Neutron Star Mass and Radius Measurements, Universe 5, p. 159.
- Lattimer, J. M. and Schutz, B. F. (2005). Constraining the Equation of State with Moment of Inertia Measurements, Ap. J. 629, pp. 979–984.
- Lavagno, A. (2010). Hot and Dense Hadronic Matter in an Effective Mean-field

- Approach, Phys. Rev. C 81, p. 044909.
- Lenka, S. S., Char, P., and Banik, S. (2017). Critical Mass, Moment of Inertia and Universal Relations of Rapidly Rotating Neutron Stars with Exotic Matter, Int. J. Mod. Phys. D 26, p. 1750127.
- Lenka, S. S., Char, P., and Banik, S. (2019). Properties of Massive Rotating Protoneutron Stars with Hyperons: Structure and universality, J. Phys. G 46, p. 105201.
- Leung, Y. C. and Wang, C. G. (1971). Properties of Hadron Matter. II. Dense Baryon Matter and Neutron Stars, Ap. J. 170, p. 499.
- Li, B.-A., Cai, B.-J., Xie, W.-J., and Zhang, N.-B. (2021). Progress in Constraining Nuclear Symmetry Energy Using Neutron Star Observables since GW170817, http://arxiv.org/abs/2105.04629 (arXiv:2105.04629 [nucl-th]).
- Li, B.-A. and Magno, M. (2020). Curvature-slope Correlation of Nuclear Symmetry Energy and its Imprints on the Crust-core Transition, Radius and Tidal Deformability of Canonical Neutron Stars, Phys. Rev. C 102, p. 045807.
- Li, J. J., Long, W. H., and Sedrakian, A. (2018a). Hypernuclear Stars from Relativistic Hartree-Fock Density Functional Theory, Eur. Phys. J. A 54, p. 133.
- Li, J. J. and Sedrakian, A. (2019a). Constraining Compact Star Properties with Nuclear Saturation Parameters, Phys. Rev. C 100, p. 015809.
- Li, J. J. and Sedrakian, A. (2019b). Implications from GW170817 for Δ-isobar Admixed Hypernuclear Compact Stars, Ap. J. Lett. 874, 2, p. L22.
- Li, J. J., Sedrakian, A., and Alford, M. (2020a). Relativistic Hybrid Stars with Sequential First-order Phase Transitions and Heavy-baryon Envelopes, Phys. Rev. D 101, p. 063022.
- Li, J. J., Sedrakian, A., and Weber, F. (2018b). Competition Between Delta Isobars and Hyperons and Properties of Compact Stars, Phys. Lett. B 783, pp. 234–240.
- Li, J. J., Sedrakian, A., and Weber, F. (2020b). Rapidly rotating Δ-resonanceadmixed Hypernuclear Compact Stars, Phys. Lett. B 810, p. 135812.
- Lombardo, U., Nozières, P., Schuck, P., Schulze, H. J., and Sedrakian, A. (2001). Transition from BCS Pairing to Bose-Einstein Condensation in Low-density Asymmetric Nuclear Matter, Phys. Rev. C 64, p. 064314.
- Lonardoni, D., Gandolfi, S., and Pederiva, F. (2013a). Effects of the Two-body and Three-body Hyperon-nucleon Interactions in Λ-hypernuclei, Phys. Rev. C 87, p. 041303.
- Lonardoni, D., Lovato, A., Gandolfi, S., and Pederiva, F. (2015). Hyperon Puzzle: Hints from quantum Monte Carlo calculations, Phys. Rev. Lett. 114, p. 092301.
- Lonardoni, D., Pederiva, F., and Gandolfi, S. (2013b). Auxiliary Field Diffusion Monte Carlo study of the Hyperon-Nucleon interaction in Λ-hypernuclei, Nucl. Phys. A 914, pp. 243–247.
- Lopes, L. L. and Menezes, D. P. (2014). Hypernuclear Matter in a Complete su(3) Symmetry Group, Phys. Rev. C 89, p. 025805.
- Margueron, J. and Gulminelli, F. (2019). Effect of High-order Empirical Param-

- eters on the Nuclear Equation of State, Phys. Rev. C 99, p. 025806.
- Margueron, J., Hoffmann Casali, R., and Gulminelli, F. (2018a). Equation of State for Dense Nucleonic Matter from Metamodeling. I. Foundational aspects, Phys. Rev. C 97, p. 025805.
- Margueron, J., Hoffmann Casali, R., and Gulminelli, F. (2018b). Equation of State for Dense Nucleonic Matter from Metamodeling. II. Predictions for neutron star properties, Phys. Rev. C 97, p. 025806.
- Margueron, J., Khan, E., and Gulminelli, F. (2017). Density Functional Approach for Multi-strange Hypernuclei: Competition between Λ and Ξ^{0,-} hyperons, Phys. Rev. C 96, 5, p. 054317.
- Marques, M., Oertel, M., Hempel, M., and Novak, J. (2017). New Temperature Dependent Hyperonic Equation of State: Application to rotating neutron star models and I-Q relations, Phys. Rev. C 96, p. 045806.
- Maselli, A., Cardoso, V., Ferrari, V., Gualtieri, L., and Pani, P. (2013). Equationof-state-independent Relations in Neutron Stars, Phys. Rev. D 88, p. 023007.
- Maslov, K. A., Kolomeitsev, E. E., and Voskresensky, D. N. (2015). Solution of the hyperon puzzle within a relativistic mean-field model, Phys. Lett. B 748, pp. 369–375.
- Maslov, K. A., Kolomeitsev, E. E., and Voskresensky, D. N. (2016). Relativistic Mean-Field Models with Scaled Hadron Masses and Couplings: Hyperons and maximum neutron star mass, Nucl. Phys. A 950, pp. 64–109.
- Massot, E., Margueron, J., and Chanfray, G. (2012). On the Maximum Mass of Hyperonic Neutron Stars, EPL 97, 3, p. 39002.
- Menezes, D. P. and Providência, C. (2017). Hyperons in the Nuclear Pasta Phase, Phys. Rev. C 96, p. 045803.
- Miller, M. C., Lamb, F. K., Dittmann, A. J., Bogdanov, S., Arzoumanian, Z., Gendreau, K. C., Guillot, S., Harding, A. K., Ho, W. C. G., Lattimer, J. M., Ludlam, R. M., Mahmoodifar, S., Morsink, S. M., Ray, P. S., Strohmayer, T. E., Wood, K. S., Enoto, T., Foster, R., Okajima, T., Prigozhin, G., and Soong, Y. (2019). PSR J0030+0451 Mass and Radius from NICER Data and Implications for the Properties of Neutron Star Matter, Ap. J. Lett 887, p. L24.
- Miller, M. C. et al. (2021). The Radius of PSR J0740+6620 from NICER and XMM-Newton Data, http://arxiv.org/abs/2105.06979 (arXiv:2105.06979 [astro-ph.HE]).
- Miyatsu, T., Cheoun, M.-K., and Saito, K. (2015). Equation of State for Neutron Stars With Hyperons and Quarks in the Relativistic Hartree-Fock Approximation, Ap. J. 813, p. 135.
- Moszkowski, S. A. (1974). Energy of Neutron-star Matter, Phys. Rev. D 9, pp. 1613–1625.
- Motta, T. F., Thomas, A. W., and Guichon, P. (2020). Do Delta Baryons Play a Role in Neutron Stars? Phys. Lett. B 80 2, p. 135266.
- Nakamura, S. X., Sato, T., Lee, T. S. H., Szczerbinska, B., and Kubodera, K. (2010). Dynamical Model of Coherent Pion Production in Neutrino-nucleus Scattering, Phys. Rev. C 81, p. 035502.

- Nakazato, K., Furusawa, S., Sumiyoshi, K., Ohnishi, A., Yamada, S., and Suzuki, H. (2012). Hyperon Matter and Black Hole Formation in Failed Supernovae, Ap. J. 745, p. 197.
- Negreiros, R., Tolos, L., Centelles, M., Ramos, A., and Dexheimer, V. (2018).
 Cooling of Small and Massive Hyperonic Stars, Ap. J. 863, p. 104.
- Nemura, H., Ishii, N., Aoki, S., and Hatsuda, T. (2007). Hyperon-nucleon Potentials from Lattice QCD, PoS LATTICE2007, p. 156.
- Nozawa, T., Stergioulas, N., Gourgoulhon, E., and Eriguchi, Y. (1998). Construction of Highly Accurate Models of Rotating Neutron Stars Comparison of three different numerical schemes, Astron. Astrophys. Suppl. Ser. 132, pp. 431–454.
- O'Connell, J. S. and Sealock, R. M. (1990). Phenomenological Δ-nucleus Potential from Inclusive Electron-nucleus Scattering Data, Phys. Rev. C 42, pp. 2290–2294.
- Oertel, M., Gulminelli, F., Providência, C., and Raduta, A. R. (2016). Hyperons in Neutron Stars and Supernova Cores, Eur. Phys. J. A 52, p. 50.
- Oertel, M., Hempel, M., Klähn, T., and Typel, S. (2017). Equations of State for Supernovae and Compact Stars, Rev. Mod. Phys. 89, p. 015007.
- Oertel, M., Providência, C., Gulminelli, F., and Raduta, A. R. (2015). Hyperons in Neutron Star Matter within Relativistic Mean-field Models, J. Phys. G 42, 7, p. 075202.
- Ono, A., Xu, J., Colonna, M., Danielewicz, P., Ko, C. M., Tsang, M. B., Wang, Y.-J., Wolter, H., Zhang, Y.-X., Chen, L.-W., Cozma, D., Elfner, H., Feng, Z.-Q., Ikeno, N., Li, B.-A., Mallik, S., Nara, Y., Ogawa, T., Ohnishi, A., Oliinychenko, D., Su, J., Song, T., Zhang, F.-S., and Zhang, Z. (2019). Comparison of Heavy-ion Transport Simulations: Collision integral with pions and Δ resonances in a box, Phys. Rev. C 100, p. 044617.
- Oppenheimer, J. R. and Volkoff, G. M. (1939). On Massive Neutron Cores, Phys. Rev. 55, pp. 374–381.
- Otto, K., Oertel, M., and Schaefer, B.-J. (2020). Nonperturbative Quark Matter Equations of State with Vector Interactions, Eur. Phys. J. 229, pp. 3629– 3649.
- Özel, F. and Freire, P. (2016). Masses, Radii, and the Equation of State of Neutron Stars, Ann. Rev. Astron. Astrophys. 54, pp. 401–440.
- Page, D. (2009). Neutron Star Cooling: I, W. Becker (ed.), Astrophysics and Space Science Library, Vol. 357 (Springer), p. 247.
- Page, D., Geppert, U., and Weber, F. (2006). The Cooling of Compact Stars, Nucl. Phys. A 777, pp. 497–530, special Issue on Nuclear Astrophysics.
- Pais, H., Bougault, R., Gulminelli, F., Providência, C., Bonnet, E., Borderie, B., Chbihi, A., Frankland, J. D., Galichet, E., Gruyer, D., Henri, M., Le Neindre, N., Lopez, O., Manduci, L., Parlôg, M., and Verde, G. (2020). Low Density In-Medium Effects on Light Clusters from Heavy-Ion Data, Physical Review Letter 125, p. 012701.
- Pandharipande, V. R. (1971). Hyperonic Matter, Nuclear Physics A 178, pp. 123–144.
- Papazoglou, P., Schramm, S., Schaffner-Bielich, J., Stoecker, H., and Greiner, W.

- (1998). Chiral Lagrangian for Strange Hadronic Matter, Phys. Rev. C 57, pp. 2576–2588.
- Peres, B., Oertel, M., and Novak, J. (2013). Influence of Pions and Hyperons on Stellar Black Hole Formation, Physical Review D 87, p. 043006.
- Potekhin, A. Y. (2010). The Physics of Neutron Stars, Physics Uspekhi 53, pp. 1235–1256.
- Potekhin, A. Y., Zyuzin, D. A., Yakovlev, D. G., Beznogov, M. V., and Shibanov, Y. A. (2020). Thermal Luminosities of Cooling Neutron Stars, Mon. Not. Roy. Astron. Soc. 496, pp. 5052–5071.
- Prakash, M., Prakash, M., Lattimer, J. M., and Pethick, C. J. (1992). Rapid Cooling of Neutron Stars by Hyperons and Delta Isobars, Ap. J. Lett. 390, p. L77.
- Providência, C., Fortin, M., Pais, H., and Rabhi, A. (2019). Hyperonic Stars and the Symmetry Energy, Frontiers in Astronomy and Space Sciences 6, p. 13.
- Providencia, C. and Rabhi, A. (2013). Interplay Between the Symmetry Energy and the Strangeness Content of Neutron Stars, Phys. Rev. C 87, p. 055801.
- Raduta, A. R. and Gulminelli, F. (2010). Statistical Description of Complex Nuclear Phases in Supernovae and Proto-neutron Stars, Phys. Rev. C 82, p. 065801
- Raduta, A. R. and Gulminelli, F. (2019). Nuclear Statistical Equilibrium Equation of State for Core Collapse, Nuclear Physics A 983, pp. 252–275.
- Raduta, A. R., Li, J. J., Sedrakian, A., and Weber, F. (2019). Cooling of hypernuclear compact stars: Hartree-Fock Models and High-density Pairing, Mon. Not. Roy. Astron. Soc. 487, pp. 2639–2652.
- Raduta, A. R., Oertel, M., and Sedrakian, A. (2020). Proto-neutron Stars with Heavy Baryons and Universal Relations, Mon. Not. Roy. Astron. Soc. 499, pp. 914–931.
- Raduta, A. R., Sedrakian, A., and Weber, F. (2017). Cooling of Hypernuclear Compact Stars, Mon. Not. R. Astron. Soc. 475, 4, pp. 4347–4356.
- Ribes, P., Ramos, A., Tolos, L., Gonzalez-Boquera, C., and Centelles, M. (2019). Interplay Between Delta Particles and Hyperons in Neutron Stars, Ap. J. 883, p. 168.
- Riek, F., Lutz, M. F. M., and Korpa, C. L. (2009). Photoabsorption off Nuclei with Self-consistent Vertex Corrections, Phys. Rev. C 80, p. 024902.
- Riley, T. E., Watts, A. L., Bogdanov, S., Ray, P. S., Ludlam, R. M., Guillot, S., Arzoumanian, Z., Baker, C. L., Bilous, A. V., Chakrabarty, D., Gendreau, K. C., Harding, A. K., Ho, W. C. G., Lattimer, J. M., Morsink, S. M., and Strohmayer, T. E. (2019). A NICER View of PSR J0030+0451: Millisecond pulsar parameter estimation, Ap. J. Lett 887, p. L21.
- Riley, T. E. et al. (2021). A NICER View of the Massive Pulsar PSR J0740+6620 Informed by Radio Timing and XMM-Newton Spectroscopy, http://arxiv. org/abs/2105.06980 (arXiv:2105.06980 [astro-ph.HE]).
- Röpke, G. (2020). Light P-shell nuclei with cluster structures ($4 \le A \le 16$) in Nuclear Matter, Phys. Rev. C **101**, p. 064310.
- Gourgoulhon, E., Grandclément, P., Marck, J.-A., Novak, J., and Taniguchi, K. (2021). LORENE Code, https://lorene.obspm.fr.

- Sahoo, H. S., Mitra, G., Mishra, R., Panda, P. K., and Li, B.-A. (2018). Neutron Star Matter with Δ Isobars in a Relativistic Quark Model, Phys. Rev. C 98, p. 045801.
- Sasaki, K. et al. (2020). ΛΛ and NΞ Interactions from Lattice QCD Near the Physical Point, Nucl. Phys. A 998, p. 121737.
- Satarov, L. M., Mishustin, I. N., Motornenko, A., Vovchenko, V., Gorenstein, M. I., and Stoecker, H. (2019). Phase Transitions and Bose-Einstein Condensation in α-nucleon Matter, Phys. Rev. C 99, p. 024909.
- Satarov, L. M., Poberezhnyuk, R. V., Mishustin, I. N., and Stoecker, H. (2021). Phase Diagram of α Matter with a Skyrme-like Scalar Interaction, Phys. Rev. C 103, p. 024301.
- Sawyer, R. F. (1972). Energy Shifts of Excited Nucleons in Neutron-star Matter, Ap. J. 176, p. 205.
- Schaab, C., Weber, F., Weigel, M. K., and Glendenning, N. K. (1996). Thermal Evolution of Compact Stars, Nucl. Phys. A 605, pp. 531–565.
- Schaffner, J. and Mishustin, I. N. (1996). Hyperon Rich Matter in Neutron Stars, Phys. Rev. C 53, pp. 1416–1429.
- Schulze, H.-J. and Rijken, T. (2011). Maximum Mass of Hyperon Stars with the Nijmegen ESC08 model, Phys. Rev. C 84, p. 035801.
- Schürhoff, T., Schramm, S., and Dexheimer, V. (2010). Neutron Stars with Small Radii The role of Δ resonances, Ap. J. **724**, 1, p. L74.
- Sedrakian, A. (2007). The Physics of Dense Hadronic Matter and Compact Stars, Prog. Part. Nucl. Phys. 58, pp. 168–246.
- Sedrakian, A. (2020). Light Clusters in Dilute Heavy-baryon Admixed Nuclear Matter, Eur. Phys. J. A 56, p. 258.
- Sedrakian, A. and Clark, J. W. (2006). Pair Condensation and Bound States in Fermionic Systems, Phys. Rev. C 73, p. 035803.
- Sedrakian, A. and Clark, J. W. (2019). Superfluidity in Nuclear Systems and Neutron Stars, Eur. Phys. J. A 55, p. 167.
- Sedrakian, A., Weber, F., and Li, J. J. (2020). Confronting GW190814 with Hyperonization in Dense Matter and Hypernuclear Compact Stars, Phys. Rev. D 102, p. 041301.
- Serot, B. D. and Walecka, J. D. (1997). Recent Progress in Quantum Hadrodynamics, Int. J. Mod. Phys. E 6, 04, pp. 515-631.
- Shahrbaf, M., Blaschke, D., and Khanmohamadi, S. (2020). Mixed Phase Transition from Hypernuclear Matter to Deconfined Quark Matter Fulfilling Massradius Constraints of Neutron Stars, J. Phys. G 47, p. 115201.
- Shahrbaf, M. and Moshfegh, H. R. (2019). Appearance of Hyperons in Neutron Stars within LOCV Method, Annals Phys. 402, pp. 66–77.
- Shapiro, I. I. (1964). Fourth Test of General Relativity, Physical Review Letter 13, pp. 789–791.
- Shapiro, S. L. and Teukolsky, S. A. (1983). Black Holes, White Dwarfs, and Neutron Stars: The physics of compact objects, ISBN 978-0-471-87316-7.
- Spinella, W. M. and Weber, F. (2020). Dense Baryonic Matter in the Cores of Neutron Stars, in: Topics on strong gravity (World Scientific), ISBN 978-981-3277-33-5, pp. 85-152.

- Stergioulas, N. (2003). Rapidly Rotating Neutron Star Code (RNS), Living Reviews in Relativity 6, Article number 3 (https://link.springer.com/article/10.12942/lrr-2003-3) (www.gravity.phys.uwm.edu/rns/).
- Taninah, A., Agbemava, S. E., Afanasjev, A. V., and Ring, P. (2020). Parametric Correlations in Energy Density Functionals, Phys. Lett. B 800, p. 135065.
- Thapa, V. B., Sinha, M., Li, J. J., and Sedrakian, A. (2020). Equation of State of Strongly Magnetized Matter with Hyperons and Δ -resonances, Particles 3, pp. 660–675.
- Thapa, V. B., Sinha, M., Li, J. J., and Sedrakian, A. (2021). Massive Δ -resonance Admixed Hypernuclear Stars with Antikaon Condensations, Phys. Rev. D 103, p. 063004.
- Togashi, H., Hiyama, E., Yamamoto, Y., and Takano, M. (2016). Equation of State for Neutron Stars with Hyperons by the Variational Method, Phys. Rev. C 93, p. 035808.
- Tolman, R. C. (1939). Static Solutions of Einstein's Field Equations for Spheres of Fluid, Phys. Rev. 55, pp. 364–373.
- Tolos, L., Centelles, M., and Ramos, A. (2016). Equation of State for Nucleonic and Hyperonic Neutron Stars with Mass and Radius Constraints, Ap. J. 834, 1, p. 3.
- Torres, J. R., Gulminelli, F., and Menezes, D. P. (2017). Examination of Strangeness Instabilities and Effects of Strange Meson Couplings in Dense Strange Hadronic Matter and Compact Stars, Phys. Rev. C 95, p. 025201.
- Tsubakihara, K. and Ohnishi, A. (2013). Three-body Couplings in RMF and its Effects on Hyperonic Star Equation of State, Nucl. Phys. A 914, pp. 438– 443
- Typel, S. (2018). Relativistic Mean-field Models with Different Parametrizations of Density Dependent Couplings, Particles 1.
- Typel, S., Röpke, G., Klähn, T., Blaschke, D., and Wolter, H. H. (2010). Composition and Thermodynamics of Nuclear Matter with Light Clusters, Phys. Rev. C 81, p. 015803.
- Typel, S. and Wolter, H. H. (1999). Relativistic Mean-field Calculations with Density-dependent Meson-nucleon Coupling, Nucl. Phys. A 656, 3-4, pp. 331–364.
- van Dalen, E., Colucci, G., and Sedrakian, A. (2014). Constraining Hypernuclear Density Functional with Λ-hypernuclei and Compact Stars, Phys. Lett. B 734, pp. 383–387.
- Vidaña, I. (2018). Hyperons: The strange ingredients of the nuclear equation of state, Proc. Roy. Soc. Lond. A 474, p. 0145.
- Viganò, D., Garcia-Garcia, A., Pons, J. A., Dehman, C., and Graber, V. (2021).
 Magneto-thermal Evolution of Neutron Stars with Coupled Ohmic, Hall and Ambipolar Effects via Accurate Finite-volume Simulations, http://arxiv.org/abs/2104.08001 (arXiv:2104.08001 [astro-ph.HE]).
- Waldhauser, B. M., Maruhn, J. A., Stöcker, H., and Greiner, W. (1987). Sensitivity of Pion Production to the Nuclear EoS and to the Delta's Coupling Constant, Z. für Phys. A Atomic Nuclei 328, 1, pp. 19–22.
- Waldhauser, B. M., Maruhn, J. A., Stöcker, H., and Greiner, W. (1988). Nuclear

- Equation of State from the Nonlinear Relativistic Mean-field Theory, Phys. Rev. C 38, pp. 1003–1009.
- Weber, F. (1999). Pulsars as Astrophysical Laboratories for Nuclear and Particle Physics, Series in High Energy Physics, Cosmology and Gravitation (Taylor & Francis), ISBN 9780750303323.
- Weber, F. and Weigel, M. (1989a). Baryon Composition and Macroscopic Properties of Neutron Stars, Nucl. Phys. A 505, 3, pp. 779 822.
- Weber, F. and Weigel, M. K. (1989b). Equation of State of Dense Baryonic Matter, J. Phys. G 15, 6, pp. 765–792.
- Wehrberger, K., Bedau, C., and Beck, F. (1989). Electromagnetic Excitation of the Delta-baryon in Quantum Hadrodynamics, Nuclear Physics A 504, pp. 797–817.
- Weissenborn, S., Chatterjee, D., and Schaffner-Bielich, J. (2012a). Hyperons and Massive Neutron Stars: The role of hyperon potentials, Nucl. Phys. A 881, pp. 62–77.
- Weissenborn, S., Chatterjee, D., and Schaffner-Bielich, J. (2012b). Hyperons and Massive Neutron Stars: Vector repulsion and SU(3) symmetry, Phys. Rev. C 85, p. 065802.
- Wu, X.-H., Wang, S.-B., Sedrakian, A., and Röpke, G. (2017). Composition of Nuclear Matter with Light Clusters and Bose-Einstein Condensation of α Particles, J. Low Temp. Phys. 189, pp. 133–146.
- Xu, J. (2019). Transport Approaches for the Description of Intermediate-energy Heavy-ion Collisions, Prog. Part. Nucl. Phys. 106, pp. 312–359.
- Yagi, K. and Yunes, N. (2017). Approximate Universal Relations for Neutron Stars and Quark Stars, Physics Reports 681, pp. 1–72.
- Yamamoto, Y., Furumoto, T., Yasutake, N., and Rijken, T. A. (2014). Hyperon Mixing and Universal Many-body Repulsion in Neutron Stars, Phys. Rev. C 90, p. 045805.
- Zdunik, J. L. and Haensel, P. (2013). Maximum Mass of Neutron Stars and Strange Neutron-star Cores, Astronomy & Astrophysics 551, p. A61.
- Zhang, N.-B. and Li, B.-A. (2019). Extracting Nuclear Symmetry Energies at High Densities from Observations of Neutron Stars and Gravitational Waves, Eur. Phys. J. A 55, 3, p. 39.
- Zhang, N.-B., Li, B.-A., and Xu, J. (2018). Combined Constraints on the Equation of State of Dense Neutron-rich Matter from Terrestrial Nuclear Experiments and Observations of Neutron Stars, Ap. J. 859, 2, p. 90.
- Zhang, Z.-W. and Chen, L.-W. (2017). Low Density Nuclear Matter with Light Clusters in a Generalized Nonlinear Relativistic Mean-field Model, Phys. Rev. C 95, p. 064330.
- Zhang, Z.-W. and Chen, L.-W. (2019). Cold Dilute Nuclear Matter with α-particle Condensation in a Generalized Nonlinear Relativistic Mean-field Model, Phys. Rev. C 100, p. 054304.
- Zhu, Z.-Y., Li, A., Hu, J.-N., and Sagawa, H. (2016). Δ(1232) Effects In Density-Dependent Relativistic HArtree-FOck Theory and Neutron Stars, Phys. Rev. C 94, p. 045803.